



HAL
open science

Rare De Novo Missense Variants in RNA Helicase DDX6 Cause Intellectual Disability and Dysmorphic Features and Lead to P-Body Defects and RNA Dysregulation

Chris Balak, Marianne Bénard, Elise Schaefer, Sumaiya Iqbal, Keri Ramsey, Michèle M. Ernoult-Lange, Francesca Mattioli, Lorida Llaci, Véronique Geoffroy, Maïté Courel, et al.

► **To cite this version:**

Chris Balak, Marianne Bénard, Elise Schaefer, Sumaiya Iqbal, Keri Ramsey, et al.. Rare De Novo Missense Variants in RNA Helicase DDX6 Cause Intellectual Disability and Dysmorphic Features and Lead to P-Body Defects and RNA Dysregulation. *American Journal of Human Genetics*, 2019, 105 (3), pp.509-525. 10.1016/j.ajhg.2019.07.010 . hal-02271087

HAL Id: hal-02271087

<https://hal.science/hal-02271087>

Submitted on 26 Nov 2020

HAL is a multi-disciplinary open access archive for the deposit and dissemination of scientific research documents, whether they are published or not. The documents may come from teaching and research institutions in France or abroad, or from public or private research centers.

L'archive ouverte pluridisciplinaire **HAL**, est destinée au dépôt et à la diffusion de documents scientifiques de niveau recherche, publiés ou non, émanant des établissements d'enseignement et de recherche français ou étrangers, des laboratoires publics ou privés.

Rare *De Novo* Missense Variants in the RNA Helicase DDX6 cause Intellectual Disability and Dysmorphic Features and Lead to P-Body Defects and RNA Dysregulation.

Chris Balak^{1,2,23,*}, Marianne Benard^{3,23}, Elise Schaefer^{4,11,23}, Sumaiya Iqbal^{5,6}, Keri Ramsey^{1,2}, Michèle Ernoult-Lange³, Francesca Mattioli^{7,8,9,10}, Lorida Llaci^{1,2}, Véronique Geoffroy¹¹, Maité Courel³, Marcus Naymik^{1,2}, Kristine K. Bachman¹², Rolph Pfundt¹³, Patrick Rump¹⁴, Johanna ter Beest¹³, Ingrid M. Wentzensen¹⁵, Kristin G. Monaghan¹⁵, Kirsty McWalter¹⁵, Ryan Richholt¹, Antony Le Béchech¹⁶, Wayne Jepsen^{1,2}, Matt De Both^{1,2}, Newell Belnap², Anne Boland¹⁷, Ignazio S. Piras^{1,2}, Jean-François Deleuze¹⁷, Szabolcs Szelinger^{1,2}, Hélène Dollfus^{4,11}, Jamel Chelly^{7,8,9,10,18}, Jean Muller^{11,18}, Arthur Campbell^{5,6}, Dennis Lal^{5,6,19,20,21}, Sampathkumar Rangasamy^{1,2}, Jean-Louis Mandel^{7,8,9,10,22}, Vinodh Narayanan^{1,2,24}, Matt Huentelman^{1,2,24}, Dominique Weil^{3,24}, Amélie Piton^{7,8,9,10,19,24,*}

1 Translational Genomics Research Institute (TGen), Neurogenomics Division, Phoenix, AZ 85004, USA

2 TGen's Center for Rare Childhood Disorders (C4RCD), Phoenix, AZ 85012, USA

3 Sorbonne Université, CNRS, Institut de Biologie Paris-Seine (IBPS), Laboratoire de Biologie du Développement, F-75005 Paris, France

4 Medical Genetics Department, University Hospitals of Strasbourg, The Institute of Medical Genetics of Alsace, 67000 Strasbourg, France

5 Stanley Center for Psychiatric Research, Broad Institute of MIT and Harvard, Cambridge, MA 02142, USA

6 Analytic and Translational Genetics Unit, Massachusetts General Hospital, Boston, MA 02114, USA

7 Institute of Genetics and Molecular and Cellular Biology, Illkirch, France

8 French National Center for Scientific Research, UMR7104, 67400 Illkirch, France

9 National Institute of Health and Medical Research U964, 67400 Illkirch, France

10 University of Strasbourg, 67081 Illkirch, France

11 Laboratoire de Génétique Médicale, Institut de génétique médicale d'Alsace, INSERM U1112, Fédération de Médecine Translationnelle de Strasbourg (FMTS), Université de Strasbourg, 67081 Strasbourg, France

12 Geisinger Medical Center, Dansville, PA 17822, USA

13 Department of Genetics, University Medical Center Groningen, University of Groningen, 9713 GZ Groningen, The Netherlands

14 Radboud University Nijmegen Medical Center, Department of Human Genetics, Division of Genome Diagnostics, 6525 GA Nijmegen, The Netherlands

15 GeneDx, Gaithersburg, MD 20877, USA

16 Medical Bioinformatics Unit, UF7363, Strasbourg University Hospital, 67000 Strasbourg, France

17 Centre National de Recherche en Génomique Humaine (CNRGH), Institut de Biologie François Jacob, CEA, Université Paris-Saclay, F-91057, Evry, France

18 Molecular Genetics Unit, Strasbourg University Hospital, 67000 Strasbourg, France

19 Epilepsy Center, Neurological Institute, Cleveland Clinic, Cleveland, OH 44195, USA

20 Genomic Medicine Institute, Lerner Research Institute Cleveland Clinic, Cleveland, OH 44195, USA

21 Cologne Center for Genomics (CCG), University of Cologne, 50931 Cologne, Germany

22 University of Strasbourg Institute of Advanced Studies, 67081 Strasbourg, France

23 These authors contributed equally to this work

24 These authors contributed equally to this work

***Correspondance:**

Amélie Piton, PhD

Laboratoire "Mécanismes génétiques des maladies neurodéveloppementales", IGBMC

Illkirch, France

Tel: +33369551652

Email: piton@igbmc.fr

Chris Balak

Translational Genomics Research Institute (TGen)

445 N. 5th Street, Phoenix, AZ 85004

Email: cbalak@tgen.org or cbalak@ucsd.edu

Key words

Intellectual disability, RNA helicase, processing bodies, p-bodies, mRNA metabolism, missense variants, DDX6, DEAD-box, DExD/H-box, helicase, RecA domain, neurodevelopmental disorder

ABSTRACT

The human RNA helicase *DDX6* is an essential component of membrane-less organelles called Processing Bodies (PBs). PBs are involved in mRNA metabolic processes including translational repression via coordinated storage of mRNAs. Previous studies in human cell lines have implicated altered *DDX6* in molecular and cellular dysfunction but clinical consequences and pathogenesis in humans have yet to be described. Here we report the identification of five rare *de novo* missense variants in *DDX6* in probands presenting with intellectual disability, developmental delay, and similar dysmorphic features including telecanthus, epicanthus, arched eyebrows, and low-set ears. All five missense variants (p.His372Arg, p.Arg373Gln, p.Cys390Arg, p.Thr391Ile and p.Thr391Pro) are located in two conserved motifs of the RecA-2 domain of *DDX6* involved in RNA binding, helicase activity, and protein-partner binding. We use functional studies to demonstrate that the first variants identified (p.Arg373Gln and p.Cys390Arg) cause significant defects in PB assembly in primary fibroblast and model human cell lines. These variants' interactions with several protein partners were also disrupted in immunoprecipitation assays. Further investigation using complementation assays included the additional variants p.Thr391Ile and p.Thr391Pro which, similarly to p.Arg373Gln and p.Cys390Arg, demonstrated significant defects in P-body assembly. Complementing these molecular findings, modeling of the variants on solved protein structures showed distinct spatial clustering near known protein binding regions. Collectively, our clinical and molecular data describe a neurodevelopmental syndrome associated with pathogenic missense variants in *DDX6*. Additionally, we suggest *DDX6* join the DExD/H-box genes *DDX3X* and *DHX30* in an emerging class of neurodevelopmental disorders involving RNA helicases.

INTRODUCTION

Intellectual disability (ID) is a result of abnormal neurodevelopment and affects at least 1% of the population. ID typically presents in the first few years of life and is characterized by impairments in cognition and adaptive behavior. It is often accompanied with further delays in language and motor skills (developmental delay, (DD)), as seen in many neurodevelopmental disorders (NDDs). Given the complexity of central nervous system development, the genetic contribution to ID is quite heterogeneous. Pathogenic variants in several hundred genes are now involved in monogenic forms of ID with each being responsible for a subset of individuals¹.

The widespread use of high-throughput sequencing has allowed for a considerable increase in the identification of these pathogenic variants. Large-scale studies utilizing whole exome sequencing (WES) or whole genome sequencing (WGS) continue to be performed looking for pathogenic *de novo* variants involved in autosomal dominant forms of ID and NDD, but have focused more on loss-of-function (LoF) variants. Hence, we can expect that most genes sensitive to LoF events will be identified in the next few years. On the contrary, identification of missense variants which lead to ID/NDD will continue for some time due to the difficulty in defining pathogenicity from large-scale sequencing data. *In silico* analyses such as spatial clustering studies will help to identify novel genes with clustered *de novo* pathogenic missense variants², but there remains a necessity for variant-specific functional studies to confidently demonstrate cellular dysfunction.

The hundreds of genes with pathogenic variants implicated in ID encode proteins involved in different neuron-specific or ubiquitous cellular processes: synaptic function and architecture, cytoskeleton remodeling, regulation of transcription/chromatin remodeling, or mRNA posttranscriptional regulation such as maturation, export, degradation, translation, etc^{1,3,4}.

In eukaryotic cells, this post-transcriptional regulation of gene expression is essential to proper neurodevelopment. A large variety of RNA-binding proteins (RBPs) control mRNA localization, translation, storage and decay in the cytoplasm, thus enabling the spatio-temporal adjustment of protein synthesis depending on cellular needs. One of the most illustrative examples of how alterations of mRNA metabolism can lead to NDD is Fragile-X syndrome, caused by pathogenic variants in the gene *FMR1*⁵, a gene encoding the FMRP protein, which is involved in regulation of mRNA transport and translation⁶.

In this study we have assembled a cohort of children with ID and other similar features who harbor rare *de novo* variants in a single exon of *DEAD-box helicase 6* (*DDX6*, MIM: 600326), a gene involved in RNA metabolism. The *DDX6* gene encodes a RNA helicase within the Helicase Superfamily 2 (SF2)⁷. SF2 helicases function on RNA in an ATP-dependent fashion. They are characterized by the presence of two RecA-like globular domains; ancient protein construction modules used in many motor-type proteins that transit on or remodel RNA/DNA, connected by a flexible linker that together forms a cleft for ATP and RNA binding. Within SF2, the DExD/H-box helicases (DEAD, DEAH, DExH and DExD) are a subfamily sharing at least eight conserved motifs and slight variations of the signature helicase motif II for which they are named. There are 50 DDX/DHX helicases in humans⁸. While most of them are functionally uncharacterized, the data available so far indicate that they have highly specific functions.

DDX6 in particular is a DEAD-box protein characterized in part by its Asp-Glu-Ala-Asp (DEAD)⁷ motif and is involved in the regulation of mRNA decay and translation⁹. It is also essential for forming cytosolic membrane-less ribonucleoprotein (RNP) granules called Processing Bodies (P-bodies, or PBs)^{10,11} which are involved in RNA metabolism through the

coordinated storage of mRNAs encoding regulatory functions^{12,13}. P-bodies are observed in all eukaryotes. Like other RNP granules, such as stress granules, germ granules, and neuronal granules, their formation relies on RNA-protein networks, multivalent low-affinity interactions and liquid-liquid phase separation. Nevertheless, each RNP granule is distinct in its composition and function. Currently, no neurological diseases have been associated with P-body defects. We present here the clinical phenotypes of individuals harboring rare *DDX6* missense variants and functional studies which indicate these variants affect *DDX6* function in terms of mRNA decay and PB assembly, leading to a neurodevelopmental *DDX6* syndrome.

SUBJECTS AND METHODS

Subjects

Whole blood, saliva, buccal cells, skin fibroblasts, and/or photos were obtained from research participants subsequent to informed consent. The research on individuals within this study was performed according to research protocols approved by the institutional review boards or local ethics committees of the Translational Genomics Research Institute (TGen) / TGen's Center for Rare Childhood Disorders (C4RCD) (Subjects 1 and 4), Strasbourg University Hospital (Subject 2) and Groningen University Medical Center / Radboud University Nijmegen Medical Center (Subject 5). All research participants and research groups, excluding Subject 5, were connected through GeneMatcher¹⁴.

DNA sequencing and bioinformatic processing

This study involves subjects and data from five unrelated families at different institutions in the US and Europe. **Subject 1** and parents underwent WES at TGen. Genomic DNA was

extracted from peripheral blood then isolated in a CLIA lab using the DNeasy extraction kit (Qiagen). Libraries were prepared with the Hyper DNA Prep Kit for Illumina Platforms (Kapa Biosystems). Exome capture was performed with the SureSelectXT Target Enrichment Platform using Clinical Research Exome baits (Agilent Technologies). Sequencing was performed by 100 base pair (bp) paired-end sequencing on a HiSeq4000 instrument (Illumina, Inc.). Reads were aligned to the human genome (Hg19/GRCh37) using the Burrows-Wheeler Aligner (BWA mem v.0.7.8)¹⁵. PCR duplicates were identified using Picard MarkDuplicates v1.79. Base quality recalibration and indel realignment were performed using the Genome Analysis Toolkit (GATK v3.5-1)¹⁶. Variants were jointly called with HaplotypeCaller and recalibrated with GATK¹⁷. Quality controls were conducted using FASTQC v0.11.5. Called variants were annotated with SnpEff v3.0a¹⁸ against Ensembl GRCh37.66 and filtered against dbSNP137 1000 Genomes Project (minor allele frequency <0.05), SnpEff Impact: High + Moderate, GATK quality score >300, and known genes. Prediction scores from dbNSFP (Database for Nonsynonymous SNP's Functional Predictions) and an internal annotation tool were used for filtering. **Subject 2** underwent a simplex WES (Dijon Hospital, Dijon, France) as previously described¹⁹. When no pathogenic variant was found, trio WGS was performed at the Centre National de Recherche en Génomique Humaine (CNRGH, Evry, France). Libraries were prepared and sequenced using the Illumina TruSeq DNA PCR-Free Library Preparation Kit and sequenced (3 lanes/genome, paired-end 100 bp) on a HiSeq2000 platform from Illumina (Illumina Inc., CA, USA) to obtain a depth of 30X for each sample. Reads were aligned on the human genome (GRCh37) using bwa software¹⁵, duplicate sequences were filtered out using Sambamba tools and an additional step of realignment was performed using GATK programs (IndelRealigner). Variants were identified using 4 programs (UnifiedGenotyper and HaplotypeCaller from GATK, Platypus²⁰ and

Samtools). Single Nucleotide Variations (SNV) falling in a coding region or in a genomic region of a known ID gene were annotated using Varank²¹ including information about the inheritance (*de novo* vs inherited variants). Comparison of SNV identified genome-wide in the proband and his parents resulted in a list of potential *de novo* variants. Structural variants were detected using SoftSV²² and copy number variants using CANOES²³ and then annotated by AnnotSV²⁴. For **Subject 4**, genomic DNA from the proband and respective parents was sequenced at GeneDx (Gaithersburg, Maryland). The exonic regions and flanking splice junctions of the genome were captured using the IDT xGen Exome Research Panel v1.0. Massively parallel (NextGen) sequencing was done on an Illumina system with 100bp or greater paired-end reads. Reads were aligned to human genome build GRCh37/hg19 and analyzed for sequence variants using a custom-developed analysis tool. Additional sequencing technology and variant interpretation protocol has been previously described²⁵. The general assertion criteria for variant classification are publicly available on the GeneDx ClinVar submission page (<http://www.ncbi.nlm.nih.gov/clinvar/submitters/26957/>). **Subject 5** and parents underwent trio WES. Sanger sequencing was used to confirm *DDX6* variants in all affected probands.

Variant prioritization and analysis

Candidate variants were categorized into inheritance patterns including *de novo*, recessive, compound heterozygous, and X-linked, and prioritized by various methods including variant frequency (less than 2% or absent) using the Genome Aggregation Database (gnomAD)²⁶. Further filtering of candidate genes and variants was performed from prediction of damaging effects using *in silico* tools such as gnomAD v2.1.1 probability of loss-of-function intolerance score (O/E, pLI) and missense Z-score, Combined Annotation Dependent Depletion

(CADD)²⁷, Genomic Evolutionary Rate Profiling (GERP)²⁸, SIFT²⁹, Polyphen 2³⁰, SNAP2³¹, Envision³², biological relevance, and association with human disorders with a neurodevelopmental phenotype in the literature. Candidate variants were interpreted using the guidelines published by the American College of Medical Genetics and Genomics (ACMG)³³.

RNA sequencing and gene expression analysis of fibroblasts

Experiments were performed in duplicate from two different fibroblast pellets obtained from S2. Total RNA was extracted using the RNeasy mini kit (Qiagen, Valencia, CA, USA) including a DNase treatment. RNA levels and quality were quantified using a Nanodrop spectrophotometer and a 2100 Bioanalyzer (Agilent, Santa Clara, CA, USA). mRNA libraries of template molecules suitable for high throughput DNA sequencing were created using TruSeq™ RNA Sample Preparation v2 Kit from 200 ng of total RNA. S2 was prepped with eight other individuals affected by Bardet Biedl syndrome or other causes of ID not related to *DDX6* mutation, and the subsequent libraries were sequenced on one run with the Illumina HiSeq 4000 sequencer as paired-end 100 base reads. Image analysis and base calling were performed using RTA 1.18.61 and CASAVA 1.8.2. Reads (403,718,870 and 299,879,030) were mapped onto the hg19 assembly of the human genome using TopHat 2.0.14 and the Bowtie 2-2.1.0 aligner. The raw sequencing data generated in the course of this RNA study are not publicly available but more details are available on demand. Gene expression was quantified using HTSeq-0.6.1³⁴ and gene annotations from Ensembl release 75. Only uniquely-mapped and non-ambiguously assigned reads were retained for further analyses. Read counts were then normalized across libraries with the median-of-ratios method proposed by Anders and Huber³⁵. To check if the normalization was correctly performed, Relative Log Expression (RLE) plots were drawn to

check that the distributions are centered around the zero line and as tight as possible. Comparisons to the eight aforementioned individuals with other neurodevelopmental or sensorineural conditions unrelated to *DDX6* mutation were performed using the statistical method proposed by Anders and Huber³⁵. The Wald test was used to estimate the p-values and they were adjusted for multiple testing with the Benjamini and Hochberg method³⁶. Significant differentially-expressed (DE) genes were analyzed using the Database for Annotation, Visualization and Integrated Discovery (DAVID 6.7). Biological processes and molecular functions of Gene Ontology Consortium (GO), as well as pathways from KEGG were used for the functional annotations. The list of genes known or suspected to be involved in ID was extracted from the SysID database (<http://sysid.cmbi.umcn.nl/>). Genes with 10 or more reads detected (on average) were considered as expressed in fibroblasts.

Molecular modeling of *DDX6* and missense variant impact prediction

High-resolution crystal structures for human *DDX6* in an open conformation (PDB ID: 4CT5) and closed conformation in complex with the CNOT1 MIF4G and 4E-T CHD domains (PDB ID: 5ANR) were obtained from Protein Data Bank originally submitted by Mathys et al³⁷ and Ozgur et al⁹. Three-dimensional (3D) mapping of gnomAD v2.1.1 missense variants and *DDX6* variants p.His372Arg, p.Arg373Gln, p.Cys390Arg, p.Thr391Pro and p.Thr391Ile were performed using PyMOL v2.1.1 and the UCSF Chimera package³⁸.

Cell Culture, siRNA, plasmids and transfection

Fibroblasts from Subject 2 and one sex-matched control individual, as well as fibroblasts from Subject 1 and her parents were maintained in 50% low glucose DMEM and 50% nutrient

mixture F10-Ham, supplemented with 10% fetal calf serum and 1% penicillin and streptomycin. Human embryonic kidney HEK293 and human epithelioid carcinoma HeLa cells were maintained in high glucose DMEM supplemented with 10% fetal calf serum and 1% penicillin and streptomycin.

To silence endogenous *DDX6*, HeLa cells were transfected using Lullaby (OZ Biosciences, Marseille, France) at the time of their plating with 0.7 µg (35 mm Petri dish) or 4.5 µg (100 mm Petri dish) of siRNA targeting the 3'UTR of *DDX6* mRNA (Eurofins Genomics, Ebersberg, Germany). The sequence of the siRNA targeting the 3'UTR of *DDX6* mRNA was: 5'-GGAACUAUGAAGACUUAAdTdT-3'¹¹. 24h later, cells were transfected with 1 µg or 5 µg of plasmid DNA (35 mm or 100 mm Petri dish, respectively) using Genjet plus DNA (SignaGen Laboratories, Rockville, USA). The c.1118G>A (p.Arg373Gln), c.1168T>C (p.Cys390Arg), c.1172C>T (p.Thr391Ile) and c.1171A>C (p.Thr391Pro) variants were introduced in the previously described FLAG-*DDX6*-HA plasmid¹⁰ using the InFusion Advantage PCR cloning kit (Clontech, Saint-Germain en Laye, France) and the following oligonucleotides (Eurofins Genomics, Ebersberg, Germany):

Arg373Gln_F: 5'-GGAACATCAAAATCGTGTATTTTCATGATTTCCGAAATGGCTTATG-3'

Arg373Gln_R: 5'-CGATTTTGATGTTCCCTGCCTCATTTTAGCATGAATATAGAAGCAA-3'

Cys390Arg_F: 5'-ATCTTGTTTCGCACTGATCTGTTTACCCGAGGTATTGATATACAAG-3'

Cys390Arg_R: 5'-CAGTGCGAACAAGATTGCGGCATAAGCCATTTTCGGAAATCATGAA-3'

Thr391Ile_F: 5'-TGTTTGCATTGATCTGTTTACCCGAGGTATTGATATACAAGCTGT-3'

Thr391Ile_R: 5'-AGATCAATGCAAACAAGATTGCGGCATAAGCCATTTTCGGAAATCA-3'

Thr391Pro_F: 5'-TTGTTTGCCCTGATCTGTTTACCCGAGGTATTGATATAACAAGCTG-3'

Thr391Pro_R: 5'-GATCAGGGCAAACAAGATTGCGGCATAAGCCATTTTCGGAAATCAT-3'. Cells were harvested 60 h after plating.

Immunofluorescence

Cells were grown on glass coverslips in 35 mm Petri dish and fixed in methanol for 3 min at -20°C. Cells were blocked 10 min in 2% BSA (bovine serum albumin) in PBS (phosphate-buffered saline), incubated 1 hour with the primary antibody, rinsed with PBS, incubated 1 hour with a fluorochoime-conjugated secondary antibody and rinsed in PBS. Slides were mounted in Citifluor (Citifluor, London, UK). For complementation assays, microscopy was performed on a Leica DMR microscope (Leica) using a 63 × 1.32 oil immersion objective. Photographs were taken using a Micromax CCD camera¹³ (Princeton Instruments) driven by the Metamorph software. For fibroblast imaging, epifluorescence microscopy was performed on an inverted Zeiss Z1 microscope (Zeiss) equipped with a motorized stage using a 63x1.4 oil immersion objective and running under the Zen software. Photographs were obtained with an Axiocam 506 mono camera (Zeiss). Images were processed with ImageJ. To quantitate PBs, we used the plugin Spot Detector of the open bioimage informatics platform Icy (<http://icy.bioimageanalysis.org>³⁹). Primary antibodies were rabbit DDX6 (Novus Biologicals, Bio-Techne, Lille, France), rabbit LSM14A (Merck-Millipore (Molsheim, France), mouse EDC4 (Santa Cruz Biotechnology, Heidelberg, Germany) and rabbit HA and mouse FLAG M2 (Sigma-Aldrich, Saint-Quentin Fallavier, France). Secondary antibodies were purchased from Jackson ImmunoResearch Laboratories (Suffolk, UK).

Immunoprecipitation and western blot analyses

For immunoprecipitation, HEK293 cells transfected with FLAG-DDX6-HA plasmids were grown in 100 mm Petri dish, washed twice in PBS, scrapped in 2 mL PBS and pelleted at 360 g. Pellets were resuspended in 0.5 mL lysis buffer (50 mM Tris pH 7.5, 125 mM NaCl, 0.5% NP40, 1mM EDTA, 1mM EGTA, 1mM DTT, 5% glycerol) supplemented with RNaseA (10 µg/mL) and 2x EDTA-free protease inhibitor cocktail (Roche Diagnostics, Meylan, France). After 30 min incubation at 4°C, nuclei were pelleted at 500 g for 10 min at 4°C, and proteins from the supernatant were immunoprecipitated as follows. 1–3 mg of the cytoplasmic extracts was incubated at 4°C for 2 h with anti-FLAG M2 magnetic beads (Sigma-Aldrich, Saint-Quentin Fallavier, France). After washing, bound proteins were eluted with SDS loading buffer. Immunoprecipitated proteins were migrated along with 30 µg of control cytoplasmic lysate and analyzed by western blot as described below. Signals were quantified from scanned X-ray films using ImageJ, normalized to the signal obtained with FLAG M2 antibody in the same experiment, and expressed as a relative percentage of binding proteins using the wild-type FLAG-tagged DDX6.

For western blot analyses, cytoplasmic extracts were prepared as described⁴⁰, except that soluble and insoluble proteins were separated by centrifugation at 500 g for 10 min at 4°C. After immunoprecipitation, proteins were separated on a NuPage 4–12% gel (Invitrogen, Thermo Fischer Scientific, Carlsbad, CA, USA) and transferred to a PVDF (poly-vinylidene fluoride) membrane (Perkin Elmer, Courtaboeuf, France). After blocking in PBS containing 5% (wt/vol) nonfat dry milk for 1 h at room temperature, the membrane was incubated with the primary antibody overnight at 4°C, rinsed in PBS, and incubated with horseradish peroxidase-conjugated secondary antibody for 1 h at room temperature. After washing in PBS, proteins were detected

using Western lightning plus ECL kit (Perkin Elmer, Courtaboeuf, France) and visualized by exposure to CL-XPosure film (Pierce, Thermo Fischer Scientific, Carlsbad, CA, USA). Primary antibodies included rabbit DDX6 (Novus Biologicals, Bio-Techne, Lille, France), rabbit ribosomal S6 (Cell Signaling Technology, Danvers, MA, USA), mouse FLAG M2 (Sigma-Aldrich, Saint-Quentin Fallavier, France), rabbit 4E-T (Abcam, Paris, France), rabbit LSM14A (Merck-Millipore, Molsheim, France), rabbit LSM14B (Sigma-Aldrich, Saint-Quentin Fallavier, France), rabbit PAT1B (Cell Signaling Technology, Danvers, MA, USA), rabbit EDC3 (Abcam, Paris, France), and mouse EDC4 (Santa Cruz Biotechnology, Heidelberg, Germany). The secondary antibodies were purchased from Jackson ImmunoResearch Laboratories (Suffolk, UK).

RESULTS

Identification of rare *de novo* missense variants in *DDX6* in individuals with ID

Individual analyses of the five families did not reveal any known pathogenic variants in genes with associated syndrome(s) closely overlapping the clinical features of the probands. Subject 1 (S1) WES study did reveal a *de novo* missense variant in a gene not previously associated to human disease, *DDX6*; NM_004397.5; c.1118G>A (p.Arg373Gln)(**Table 1**). Data also showed compound heterozygous missense variants of unknown significance (VUS) in *DNAH11* (MIM: 603339) (**Table S1**). *DNAH11* is associated with autosomal recessive Ciliary Dyskinesia, Primary, 7, with or without *situs inversus* (CILD7) (MIM: 611884) predominately through LoF mutations. Clinical features of CILD7 do not include ID or resemble S1's phenotype. Further, *DNAH11* possesses significantly more missense variation than expected in gnomAD (Z -score = -5.61) and ClinVar contains no confirmed pathogenic missense variants.

Thus, the VUS was excluded as a candidate. Subject 2 (S2) first underwent an ID gene panel sequencing, singleton WES, and finally WGS of the nuclear family. Among the 146 putative *de novo* variants identified in the proband, only one occurred in a coding region: a missense change c.1168T>C (p.Cys390Arg) in *DDX6*. No other candidate variant(s) were identified in coding or genomic regions of genes known to be involved in ID. Two additional *de novo* missense variants in *DDX6*, c.1172C>T (p.Thr391Ile)(Subject 3, S3) and c.1171A>C (p.Thr391Pro)(Subject 4, S4), were identified by trio WES in unrelated individuals with developmental disorders (GeneDx). Subject 4 carries an additional hemizygous missense VUS in the gene *SLC16A2* (MIM: 30095) associated with Allan-Herndon-Dudley syndrome (AHDS, MIM: 300523), but this diagnosis does not fit with his clinical history (**Table S1**). A key feature of males with AHDS is abnormal triiodothyronine (T3) and thyroxine (T4) levels. Repeat thyroid studies in S4 including dosages of T3 and T4 (free, total, and reverse) in S4 were all normal. During the final stages of this study, a fifth individual (Subject 5, S5) with a single *de novo* missense variant c.1115A>G (p.His372Arg) in *DDX6* was identified by WES. For all individuals, no other variants except the *DDX6* missense changes described above were classified pathogenic or likely pathogenic according to ACMG guidelines.

Clinical features of individuals carrying *de novo* missense variants in *DDX6* exon 11

We could retrieve clinical information for four of the individuals carrying *de novo* missense variants in *DDX6*. These probands are from unrelated families in both the USA and Europe. The affected individuals present with NDD of unknown etiology and range between the ages of 4 to 13 years at last clinical assessment. Parents are noted to be without any significant health problems. Phenotyping of the four affected probands showed overlap of clinical features

and minor variation in severity across individuals (**Table 2**). Clinical features include ID (4/4), DD (4/4), mild/moderate cardiac anomalies (3/4), hypotonia (3/4), gait instability (3/4), hand/feet and genitourinary abnormalities (3/4). Other features present include mild-moderate MRI anomalies, small head circumference (<-2 Standard Deviations SD), congenital hydronephrosis with vesicoureteral reflux, mild obesity, and autistic traits. The probands also share common facial dysmorphic features including a high forehead, a bulbous nasal tip, widely-spaced eyes, arched eyebrows and low-set ears (**Figure 1**). Expanded summaries can be found in Supplemental Data: Case Reports.

***DDX6* missense variants found in affected individuals are absent from population databases, evolutionarily conserved, and spatially clustered within protein**

All *de novo* missense variants identified in affected individuals are located in exon 11 of *DDX6*. This exon is present in all *DDX6* isoforms and codes for conserved motifs QxxR and V within the second RecA-2 domain of the helicase core. The variants have not been observed in the gnomAD database, which contains genetic data from ~140 thousand individuals and is depleted of severe pediatric disorders. *DDX6* is highly intolerant to LoF variants as indicated by gnomAD's (v2.1.1) observed/expected LoF ratio of 0.04 (confident interval [0.01-0.17]), with only one heterozygous LoF change reported in the penultimate exon of its canonical isoform (NM_004397.5). *DDX6* was also found to have significant intolerance to missense change indicated by a gnomAD Z-score of 3.93 (observed/expected ratio of 0.34 [0.29-0.41]) suggesting selection pressure against amino acid changes²⁶. In particular, exon 11 (aa 371-391) was found highly depleted of nonsynonymous variations in gnomAD (**Figure 2A**). The specific variants identified in probands lead to changes at conserved positions and are predicted to be deleterious

by *in silico* analysis tools (**Table 1, Figure 2B**). The QxxR motif containing Arg373 is conserved in 33/35 DEAD-box family members, with the varying residues being structurally and chemically similar (Glutamine). In Motiv V, residue 390 maintains small, uncharged residues throughout the DEAD-box protein family (35/35), and Thr391 is conserved in every member (**Figure S1, Figure S2**). Further, mapping of the variants on a 3D structure of DDX6 in complex with the CNOT1 MIF4G and 4E-T CHD domains³⁷ showed proband variants spatially cluster near or at the protein surface in a region depleted of missense variants in gnomAD populations (**Figure 2C-D**) and close to the 4E-T interaction surface, suggesting that this region is of functional importance for DDX6.

Mutant DDX6 proteins are defective in PB assembly

As DDX6 is known to be involved in the formation of cytoplasmic PBs, we first analyzed the presence of PBs in fibroblasts obtained from S2 carrying the p.Cys390Arg change and from an unrelated age-matched control subject. Cells were analyzed by immunofluorescence using antibodies against DDX6 and a second PB marker, EDC4 (**Figure 3A**). While most fibroblasts from the control subject showed numerous PBs detected by both DDX6 and EDC4 antibodies, only some of the fibroblasts obtained from S2 contained PBs. However, Western blot analyses indicated that similar amount of DDX6 protein was present in these cells (**Figure S3A, 3C**), suggesting a functional defect in this variant. Fibroblasts were also obtained from S1 carrying the p.Arg373Gln variant and from her parents. Again, Western blot analysis showed similar levels of DDX6 protein in the three cell samples (**Figure S3A**), while immunostaining indicated that the proband's cells contained fewer PBs than the mother's ones (**Figure S3B-S3C**). The father's cells grew slowly however, and possibly related to that, had an intermediate number of PBs:

lower than the mother's, but higher than S1's cells (**Figure S3B, S3C**). To confirm the specific defect of PBs in S1, we therefore submitted the three cell cultures to a mild cold shock at 30°C for 2 hours, since we showed previously that such a treatment results in increased number and size of PBs in established cell lines¹⁰. With this treatment, 90% of the parents' cells contained numerous PBs, while 70% of S1's cells remained devoid of PBs (**Figure 3B, 3C**). Moreover, in the 30% of cells with PBs, their numbers remained low, thus confirming a specific PB defect in the proband cells.

We then investigated the ability of the different variant-containing DDX6 proteins to assemble PBs in a model human cell line¹¹. Plasmids encoding the four DDX6 variants initially identified (p.Arg373Gln, p.Cys390Arg, p.Thr391Ile, and p.Thr391Pro) fused to FLAG and HA tags were transfected in HeLa cells (**Figure S4A**). The variant proteins localized in PBs, as assessed by immunofluorescence using LSM14A as a P-body marker (**Figure S4B**). However, they dramatically affect PB assembly as tested by the following complementation assay (**Figure 4A**). Briefly, cells were depleted of endogenous DDX6 by using siRNA targeting the 3'UTR of *DDX6* mRNA (**Figure 4B**), which resulted as expected¹¹ in PB disassembly (**Figure 4A, 4C**). 24 h later, cells were transfected with wild-type or mutant FLAG-DDX6-HA plasmids and analyzed 40 h later for the presence of PBs (**Figure 4A, 4C**). Whereas the wild-type DDX6 restored PB assembly, no or very few PBs were observed using the mutant proteins, with less than 5% efficiency for p.Arg373Gln, p.Cys390Arg and p.The391Ile variants as compared to the wild-type protein, and 17% for the p.Thr391Pro variant (**Figures 4A, 4C**). Similar results were obtained using EDC4 as a PB marker (**Figure S4C**). This indicated that the mutant DDX6 proteins were unable to replace the endogenous DDX6 for PB formation.

Mutant DDX6 proteins are defective in interactions with protein partners key to PB assembly.

Previously, we showed that three factors, DDX6, LSM14A and 4E-T, are required and their interactions essential for PB assembly^{10,11,41}. Mutating the DDX6 FDF-binding pocket (Mut1: four substitutions introduced between residues 320 and 331^{9,42,43}) prevents the binding of LSM14A and 4E-T and strongly reduces PB formation¹⁰. Since the variants identified in *DDX6* are located close to the Mut1 mutations, we hypothesized that they could also alter interactions between DDX6 and these protein partners. To address this question, plasmids encoding wild-type and mutant DDX6 (p.Arg373Gln and p.Cys390Arg) fused to FLAG and HA were transfected in HEK293 cells after depletion of the endogenous DDX6 protein, immunoprecipitated 48 hours later with FLAG antibodies, and protein complexes were analyzed by western blot (**Figure 4D**). First, both mutant DDX6 proteins showed reduced binding to 4E-T and LSM14A, as compared to wild-type DDX6, and the defect was stronger for p.Arg373Gln than for the p.Cys390Arg mutant. This is consistent with the inability of these mutants to assemble PBs in the complementation assay. A binding defect was also observed for other DDX6 partners: LSM14B binding was as affected as LSM14A with both mutants, while other bindings were defective only in the case of the p.Arg373Gln mutant. This included a strong defect in PAT1B binding and some impairment of EDC3 and EDC4 binding as well. Overall, the p.Arg373Gln mutant protein was the most defective for interacting with its partners, especially those acting as translation repressors (LSM14A, 4E-T, PAT1B).

p.Cys390Arg variant cells accumulate mRNAs involved in translational regulation, DDX6 mRNA targets, and PB-excluded mRNAs.

Transcriptomic (RNAseq) analysis was performed from skin fibroblasts obtained from S2 (carrying the p.Cys390Arg variant) and compared to eight unrelated individuals with other neurodevelopmental or sensorineural conditions unrelated to *DDX6* mutation. More than one thousand genes were found to be significantly (p-adjusted <0.05) differentially expressed (DE) (**Figure 5A**) including 493 up-regulated and 979 down-regulated protein-coding genes (**Table S2**). Enrichment analysis using DAVID⁴⁴ demonstrated that the set of genes significantly upregulated was enriched for Gene Ontology Biological Process and Molecular Function terms related to protein translation such as “SRP-dependent cotranslational membrane targeting” (GO:0006614, fold enrichment FE=12.5, adjusted p-value=2.0e-18) or “formation of translation preinitiation complex” (GO:0001731, FE=11.3, adjusted p-value=3.3e-02), or “structural component of the ribosome” (GO003735, FE=5.4, adjusted p-value=1.5e-9) (**Figure 5B**). This enrichment was confirmed by analyzing KEGG pathways (“ribosome”, map03010 FE=7.9, adjusted p-value=7.2e-15). More specifically, 4 out of the 14 expressed eIF3 translation initiation factor subunit mRNAs and 28 of the 85 expressed ribosomal protein mRNAs were significantly up-regulated in S2, whereas none were significantly depleted (**Table S3**). A subset of the DE genes encode RNA-binding proteins also known to be involved in ID (*CNOT3*, *HNRNPH2*, *DDX59*, *RPL10*, etc.) (**Table S4**).

To investigate relationships between S2’s transcriptomic profile and *DDX6* function, we took advantage of two datasets available from the ENCODE project, both from the human erythroid cell line K562: 1) a *DDX6* cross-linking followed by immunoprecipitation (CLIP) experiment identifying mRNAs that bind to *DDX6* and 2) a transcriptome after induction of a stably-transfected *DDX6* shRNA for 48 hours identifying mRNAs differentially expressed after *DDX6* silencing. If the *DDX6*-Cys390Arg variant leads to a defect in its function in mRNA

decay, we would expect an accumulation of these DDX6 mRNA targets. Indeed, we first observed that significantly enriched mRNAs in S2 fibroblasts were also enriched in ENCODE's DDX6 CLIP experimental data (**Figure 5C, left panel**), indicating their direct binding to DDX6. Second, S2-enriched mRNAs also tended to be enriched in the DDX6-silencing dataset (**Figure 5C, right panel**). Thus, in spite of the differences between the two cell types under comparison (dermal fibroblasts producing a p.Cys390Arg^{+/-} variant DDX6 versus an immortalized erythroid cell line transiently depleted for DDX6); there was a common signature of enriched mRNAs between the two. Further, the enrichment was even stronger for the mRNA subset that was enriched in both the CLIP experiments and the DDX6 silencing experiment (**Figure 5C, right panel**), indicating that the mRNAs enriched in the cells of S2 were likely decayed by a DDX6-dependent mechanism that involved direct DDX6 binding.

We have recently shown that mRNAs regulated by DDX6 at the level of decay are localized out of PBs¹². Accordingly, comparing S2's transcriptome to the mRNA content of purified PBs showed that mRNAs which are enriched in S2's fibroblasts are excluded from PBs (**Figure 5D**). In the same study we showed that the mRNAs targeted to PBs, in contrast, are regulated at the level of translation. While translation regulation is not accessible in our transcriptome analysis, the fact that PBs are drastically reduced in S2 strongly suggests that DDX6-dependent translation repression is also affected in these cells. Finally, the mRNAs accumulating in S2 have a high GC content compared to other human genes, whereas the mRNAs depleted are rather AU-rich (**Figure 5E**). This is consistent with our recent study showing that DDX6 is preferentially involved in the decay of GC-rich mRNAs. Such a high GC content increases the frequency of optimal codons and is therefore observed in actively translated mRNAs.

DISCUSSION

In this study, we describe five rare *de novo* missense variants in the RNA helicase *DDX6*, identified in individuals with intellectual disability (ID). Clinical, genetic, and functional data demonstrated that these missense variants, inducing deficits in *DDX6* functions, cause an autosomal-dominant form of intellectual disability associated with mild dysmorphic features. These deficits include *DDX6* ability to assemble PBs - constitutive cytoplasmic RNP granules which act in mRNA storage - resulting in their drastic reduction in primary cells of affected individuals as well as when modeled in human cell lines. Furthermore, co-immunoprecipitation assays showed the pathogenic variants affect *DDX6* interactions with protein partners involved in PB assembly, such as LSM14A and 4E-T, suggesting a mechanism for PB dysfunction and subsequent deregulation of mRNA storage. Interactions with other *DDX6* protein partners (PAT1B, EDC3, and EDC4) were differently impacted, depending on the variants. The surface of *DDX6* that interacts with these different proteins was reported to be distinct, though overlapping. Therefore, we did not expect that different variants of *DDX6* would alter all interactions to the same extent. Additional defects included *DDX6* dysfunction in the control of mRNA stability, since transcriptomic analysis of S2 revealed an enrichment of mRNAs that are regulated by *DDX6* at the level of decay⁴⁵ (**Figure 5F**). This includes in particular mRNA encoding subunits of the translation initiation factor eIF3 and ribosomal proteins. Many also contain a TOP motif in their 5' UTR responsible for their control by the mTORC1 kinase (25 out of the 94 TOP mRNAs previously reported⁴⁶ were enriched in S2 cells). Their deregulation could have consequences on the control of cell proliferation/function inside and outside of the CNS^{46,47}. Taken together, these findings highlight crucial roles for *DDX6* and/or PBs in proper neurodevelopment.

The missense changes identified in affected individuals cluster in two pairs of amino acids in conserved motifs of the *DDX6* C-terminal RecA domain: residues 372-373 which comprise the second half of the QxxR motif, and 390-391 which lie in motif V⁴⁸ (**Figure 2A, Figure S1**). The substitutions p.Arg373Gln (S1) and p.His372Arg (S5) cause significant alterations to residue properties and likely the local structure/function. Electrically-charged surface residues like Arg373 are known to promote proper protein folding through solvent interactions, and reactive histidines are most common in protein active sites. The QxxR motif is also involved in interdomain interactions with motif Ia *in vitro* in the yeast DEAD-box protein Mss116p⁴⁹, which was proposed to help form a continuous RNA binding surface and stabilize bound RNA. The substitution of Cys390 (S2) to a large electrically-charged arginine, and the conversions of Thr391 (S3,S4) from a polar threonine to non-polar, unreactive residues (proline/isoleucine), also suggest destabilizing regional changes to the RecA-2 domain. Our co-immunoprecipitation and complementation assays support these predictions with results showing dysfunction of the variant *DDX6* proteins to bind partners through this region and to assemble PBs, respectively. Since the proband fibroblasts have a strong PB deficiency despite the presence of one wild-type allele, it raises the possibility that the *DDX6* variants could have some dominant-negative effect on PB assembly. We have previously characterized a clearly dominant-negative *DDX6* change in *DDX6* (motif VI mutant HRIG) in an experiment similar to the one described here (**Figure S4B**) and found that its expression completely suppressed PBs in the presence of the endogenous *DDX6* protein¹¹, which is not the case for the probands' variants. We would therefore favor the hypothesis that the low PB assembly results from haploinsufficiency of the wild-type allele.

DDX6 is not the first gene encoding a RNA helicase involved in monogenic forms of NDD/ID. The involvement of *DHX30* in ID was uncovered in 2017 with several *de novo* missense variants also in the RecA domains reported in twelve individuals with ID, speech impairment and gait abnormalities⁵⁰. Pathogenic variants including *de novo* truncating and missense changes in RecA domains were have also been recently reported in the *DDX3X* gene⁵¹, located on the X-chromosome, in females with ID, hypotonia, movement disorders, and epilepsy. *DDX3X* now represents one of the genes most frequently mutated in ID; involved in ~0.5% of ID cases and ~2% of female cases⁵². Interestingly, after sequence alignment of *DDX6* and *DDX3X*, the Arg373 position found mutated in our cohort corresponds to the Arg480 position recurrently mutated in the *DDX3X* cohort of affected individuals, reinforcing the functional importance of this amino acid and the QxxR motif in DEAD-box proteins. LoF function variants in another member of this helicase family, *DDX59*, have also been reported to cause an autosomal recessive form of ID with features of oral-facial-digital syndrome⁵³⁻⁵⁵.

Interestingly, the phenotypic traits observed in our *DDX6* cohort align well with the syndromes described in individuals with pathogenic variants in *DDX3X* and *DHX30*⁵⁰⁻⁵². These include ID/DD, movement/gait problems, cardiac anomalies, and corpus callosum hypoplasia as well as dysmorphic facial features (high forehead, bulbous nasal tip, hypertelorism, and arched eyebrows). Conversely, none of the individuals with *DDX6* variants have reported seizures, a feature present in the *DDX3X* and *DHX30* syndromes. This could be an interesting delineation of the *DDX6* cohort and give specific biological insights into the specificity of each DExD/H-box protein. However, seizures are present in only a subset of the *DDX3X* and *DHX30* cohorts (~16% and 25%, respectively), thus more individuals with *DDX6* syndrome are needed to completely exclude seizures as an absent feature. Our cohort also exhibits a degree of variability in their

clinical presentations. Individuals S1 and S5 present with mild abnormalities on brain MRI (corpus callosum hypoplasia) and appear to be slightly more affected than the others. Their amino acid changes (p.His372Arg and p.Arg373Gln) lie in the QxxR motif suggesting variants in this motif elicit a slightly more severe phenotype than variants in the motif V region. In support of this, co-immunoprecipitation studies demonstrated more drastic defects of protein binding caused by the p.Arg373Gln variant. Since differences in the proband's genetic backgrounds are also likely to contribute to phenotypic variability, more individuals with pathogenic *DDX6* variation will be required to fully answer this question.

DDX6 is widely expressed throughout tissues with some of the highest levels in the cerebellar hemispheres. Its expression is timely regulated in the mouse neocortex during development⁵⁶, and it has been found to be expressed in both mouse⁵⁷ and human neural stem cells (NSCs) (data extracted from previous works⁵⁸). *DDX6* is further involved in the CNS as it increases the activity of Let-7a, a microRNA important in neuronal differentiation. *DDX6* overexpression in mouse NSCs leads to an increase in neuronal differentiation whereas loss of *DDX6* function inhibits the formation of new neurons⁵⁷. *DDX3X* was also found to be essential for neuronal differentiation and migration, and its inactivation in mice disturbs cortex development and leads to abnormal distribution of neurons in the cortical plate⁵⁹. It is possible the brain anomalies present in *DDX6* individuals S1 and S5 result from impaired processes in NSC specification. While some evidence supports this idea, the exceedingly heterogeneous nature of corpus callosum anomalies requires further *in-vivo* work to validate how these pathogenic variants would alter proliferation/differentiation/migration of neuronal precursors and synaptic functioning, and also to identify which mRNAs are deregulated in this cell type.

We have shown that our *DDX6* variants result in failure to form PBs efficiently and lead to a decreased number of these RNP granules in fibroblasts of affected individuals. Lessel et al. recently showed that *DHX30* missense variants, in addition to altering DHX30 ability to bind RNA or to exert its ATPase activity, increase the formation of another significant type of RNP granules, stress granules, which is associated with a decrease of global protein translation⁵⁰. The missense variants identified in *DDX3X* were also shown to affect ATPase helicase activity and lead to protein accumulation into RNP granules not well characterized but harboring some translational activity⁵⁹. RNP granule dysfunction in neurons specifically could relate to their polar, asymmetric nature. Indeed, there are a variety of neuronal RNP granules, mostly described in dendrites. Several types of dendritic granules contain PB components, and were initially called P-body-like structures⁶⁰ or P-bodies⁶¹. They are important in regulating local translation at the synapse, which is essential for synaptic plasticity⁶². However, further attempts to define these granules with expression of DDX6 and decapping enzymes suggested that these structures were more diverse in neuronal processes than in other cells⁶³. In the neuronal soma, RNP granules may be closer to fibroblast PBs in terms of composition and function, but they have not been well characterized. Repression by miRNAs also plays a major role in the control of signaling pathways regulating several steps of cortical development⁶⁴, therefore we can speculate that the different cytoplasmic foci that play roles in the storage of miRNA targets are important for a proper development of the brain.

The present study has taken effort to demonstrate rare changes in *DDX6* cause PB and mRNA metabolism dysfunction. These DDX6 dysfunctions were observed not only by overexpressing DDX6 in immortalized cell lines but also directly in affected individual's primary fibroblasts (individuals S1 and S2). The use of these non-neuronal cells may only

Pdistantly reflect the actual disease pathogenesis in affected individual's brains and other organs. Further transcriptomic and proteomic studies in neuronal cells derived from primary fibroblasts or *in-vivo* animal models will shine more light on the specific mechanisms of DDX6-associated pathogenesis in neurodevelopment.

In conclusion, our findings implicate rare *de novo* missense variants in the second RecA domain of *DDX6* in a neurodevelopmental disorder (NDD) with ID. These variants significantly affect DDX6's ability to assemble PBs, resulting in their drastic reduction in cells, and, in our affected individual with transcriptomic data, the significant alteration of the transcriptome landscape. We suggest rare variants in *DDX6* be considered for pathogenicity in pediatric cases of NDDs with ID and this RNA helicase be added to the growing list of ID/NDD genes. Lastly, together with the recent involvement of *DDX3X* and *DHX30* in ID and similar NDDs, these results also highlight an emerging class of NDD involving RNA helicases.

SUPPLEMENTAL DATA

Supplemental Data include four figures, four tables, and expanded clinical descriptions of the subjects.

ACKNOWLEDGEMENTS

The authors thank the families for their participation to the study. The authors also thank the Foundation Jerome Lejeune and Fondation Maladies Rares for their financial support, as well as the Association Paul and Liba Mandel and the CREGEMES. This study was also supported by the grant ANR-10-LABX-0030-INRT, a French State fund managed by the Agence Nationale de la Recherche under the frame program Investissements d'Avenir ANR-10-IDEX-0002-02, the

ANR grant 14-CE09-0013-01ANR, and the Laboratory of Excellence GENMED (Medical Genomics) grant no. ANR-10-LABX-0013 managed by the National Research Agency (ANR) part of the Investment for the Future program. The authors want also to thank all the people from IGBMC sequencing platform (Bernard Jost, Christelle Thibaut-Charpentier, Céline Keime, Damien Plassard) for their technical and bioinformatics support. The authors would like to thank all donors who have contributed and participated in TGen's Center for Rare Childhood Disorders Center. Lastly, the authors thank all of the families for their participation in this study.

DECLARATION OF INTERESTS

IW, KGM, KM are employees of GeneDx, Inc.

WEB RESOURCES

The URLs for online tools and data presented herein are:

Clinvar: <http://www.ncbi.nlm.nih.gov/clinvar/>

dbSNP: <http://www.ncbi.nlm.nih.gov/projects/SNP/>

Decipher: <https://decipher.sanger.ac.uk/>

ENCODE: <https://www.encodeproject.org/>

ExAC Browser (Beta) | Exome Aggregation Consortium: <http://exac.broadinstitute.org/>

GnomAD Exome Variant Server: <http://gnomad.broadinstitute.org/>

GeneMatcher: <https://genematcher.org/>

Integrative Genomics Viewer (IGV): <http://www.broadinstitute.org/igv/>

Mutation Nomenclature: <http://www.hgvs.org/mutnomen/recs.html>

OMIM: <http://www.omim.org/>

UCSC: <http://genome.ucsc.edu/>

SNAP2: <https://roslab.org/services/snap2web/>

Protein Data Bank (PDB) : <http://www.pdb.org>

REFERENCES

1. Vissers, L.E.L.M., Gilissen, C., and Veltman, J.A. (2016). Genetic studies in intellectual disability and related disorders. *Nat. Rev. Genet.* *17*, 9–18.
2. Lelieveld, S.H., Wiel, L., Venselaar, H., Pfundt, R., Vriend, G., Veltman, J.A., Brunner, H.G., Vissers, L.E.L.M., and Gilissen, C. (2017). Spatial Clustering of de Novo Missense Mutations Identifies Candidate Neurodevelopmental Disorder-Associated Genes. *Am. J. Hum. Genet.* *101*, 478–484.
3. Bardoni, B., Abekhouk, S., Zongaro, S., and Melko, M. (2012). Intellectual disabilities, neuronal posttranscriptional RNA metabolism, and RNA-binding proteins: three actors for a complex scenario. *Prog. Brain Res.* *197*, 29–51.
4. Sartor, F., Anderson, J., McCaig, C., Miedzybrodzka, Z., and Müller, B. (2015). Mutation of genes controlling mRNA metabolism and protein synthesis predisposes to neurodevelopmental disorders. *Biochem. Soc. Trans.* *43*, 1259–1265.
5. Oberlé, I., Rousseau, F., Heitz, D., Kretz, C., Devys, D., Hanauer, A., Boué, J., Bertheas, M.F., and Mandel, J.L. (1991). Instability of a 550-base pair DNA segment and abnormal methylation in fragile X syndrome. *Science* *252*, 1097–1102.
6. Hagerman, R.J., Berry-Kravis, E., Hazlett, H.C., Bailey, D.B., Moine, H., Kooy, R.F., Tassone, F., Gantois, I., Sonenberg, N., Mandel, J.L., et al. (2017). Fragile X syndrome. *Nat Rev Dis Primers* *3*, 17065.
7. Jankowsky, E., and Fairman, M.E. (2007). RNA helicases--one fold for many functions. *Curr. Opin. Struct. Biol.* *17*, 316–324.
8. Abdelhaleem, M., Maltais, L., and Wain, H. (2003). The human DDX and DHX gene families of putative RNA helicases. *Genomics* *81*, 618–622.
9. Ozgur, S., Basquin, J., Kamenska, A., Filipowicz, W., Standart, N., and Conti, E. (2015). Structure of a Human 4E-T/DDX6/CNOT1 Complex Reveals the Different Interplay of DDX6-Binding Proteins with the CCR4-NOT Complex. *Cell Rep* *13*, 703–711.
10. Ayache, J., Bénard, M., Ernoult-Lange, M., Minshall, N., Standart, N., Kress, M., and Weil, D. (2015). P-body assembly requires DDX6 repression complexes rather than decay or Ataxin2/2L complexes. *Mol. Biol. Cell* *26*, 2579–2595.
11. Minshall, N., Kress, M., Weil, D., and Standart, N. (2009). Role of p54 RNA helicase activity and its C-terminal domain in translational repression, P-body localization and assembly. *Mol. Biol. Cell* *20*, 2464–2472.

12. Hubstenberger, A., Courel, M., Bénard, M., Souquere, S., Ernoult-Lange, M., Chouaib, R., Yi, Z., Morlot, J.-B., Munier, A., Fradet, M., et al. (2017). P-Body Purification Reveals the Condensation of Repressed mRNA Regulons. *Mol. Cell* *68*, 144-157.e5.
13. Standart, N., and Weil, D. (2018). P-Bodies: Cytosolic Droplets for Coordinated mRNA Storage. *Trends Genet.* *34*, 612–626.
14. Sobreira, N., Schiettecatte, F., Valle, D., and Hamosh, A. (2015). GeneMatcher: a matching tool for connecting investigators with an interest in the same gene. *Hum. Mutat.* *36*, 928–930.
15. Li, H., and Durbin, R. (2009). Fast and accurate short read alignment with Burrows-Wheeler transform. *Bioinformatics* *25*, 1754–1760.
16. McKenna, A., Hanna, M., Banks, E., Sivachenko, A., Cibulskis, K., Kernytsky, A., Garimella, K., Altshuler, D., Gabriel, S., Daly, M., et al. (2010). The Genome Analysis Toolkit: a MapReduce framework for analyzing next-generation DNA sequencing data. *Genome Res.* *20*, 1297–1303.
17. Van der Auwera, G.A., Carneiro, M.O., Hartl, C., Poplin, R., Del Angel, G., Levy-Moonshine, A., Jordan, T., Shakir, K., Roazen, D., Thibault, J., et al. (2013). From FastQ data to high confidence variant calls: the Genome Analysis Toolkit best practices pipeline. *Curr Protoc Bioinformatics* *43*, 11.10.1-33.
18. Cingolani, P., Platts, A., Wang, L.L., Coon, M., Nguyen, T., Wang, L., Land, S.J., Lu, X., and Ruden, D.M. (2012). A program for annotating and predicting the effects of single nucleotide polymorphisms, SnpEff: SNPs in the genome of *Drosophila melanogaster* strain w1118; iso-2; iso-3. *Fly (Austin)* *6*, 80–92.
19. Thevenon, J., Duffourd, Y., Masurel-Paulet, A., Lefebvre, M., Feillet, F., El Chehadeh-Djebbar, S., St-Onge, J., Steinmetz, A., Huet, F., Chouchane, M., et al. (2016). Diagnostic odyssey in severe neurodevelopmental disorders: toward clinical whole-exome sequencing as a first-line diagnostic test. *Clin. Genet.* *89*, 700–707.
20. Rimmer, A., Phan, H., Mathieson, I., Iqbal, Z., Twigg, S.R.F., WGS500 Consortium, Wilkie, A.O.M., McVean, G., and Lunter, G. (2014). Integrating mapping-, assembly- and haplotype-based approaches for calling variants in clinical sequencing applications. *Nat. Genet.* *46*, 912–918.
21. Geoffroy, V., Pizot, C., Redin, C., Piton, A., Vasli, N., Stoetzel, C., Blavier, A., Laporte, J., and Muller, J. (2015). VaRank: a simple and powerful tool for ranking genetic variants. *PeerJ* *3*, e796.
22. Bartenhagen, C., and Dugas, M. (2016). Robust and exact structural variation detection with paired-end and soft-clipped alignments: SoftSV compared with eight algorithms. *Brief. Bioinformatics* *17*, 51–62.
23. Backenroth, D., Homsy, J., Murillo, L.R., Glessner, J., Lin, E., Brueckner, M., Lifton, R., Goldmuntz, E., Chung, W.K., and Shen, Y. (2014). CANOES: detecting rare copy number variants from whole exome sequencing data. *Nucleic Acids Res.* *42*, e97.
24. Geoffroy, V., Herenger, Y., Kress, A., Stoetzel, C., Piton, A., Dollfus, H., and Muller, J. (2018). AnnotSV: an integrated tool for structural variations annotation. *Bioinformatics* *34*, 3572–3574.

25. Tanaka, A.J., Cho, M.T., Retterer, K., Jones, J.R., Nowak, C., Douglas, J., Jiang, Y.-H., McConkie-Rosell, A., Schaefer, G.B., Kaylor, J., et al. (2016). De novo pathogenic variants in CHAMP1 are associated with global developmental delay, intellectual disability, and dysmorphic facial features. *Cold Spring Harb Mol Case Stud* 2, a000661.
26. Lek, M., Karczewski, K.J., Minikel, E.V., Samocha, K.E., Banks, E., Fennell, T., O'Donnell-Luria, A.H., Ware, J.S., Hill, A.J., Cummings, B.B., et al. (2016). Analysis of protein-coding genetic variation in 60,706 humans. *Nature* 536, 285–291.
27. Kircher, M., Witten, D.M., Jain, P., O'Roak, B.J., Cooper, G.M., and Shendure, J. (2014). A general framework for estimating the relative pathogenicity of human genetic variants. *Nat. Genet.* 46, 310–315.
28. Cooper, G.M., Stone, E.A., Asimenos, G., NISC Comparative Sequencing Program, Green, E.D., Batzoglou, S., and Sidow, A. (2005). Distribution and intensity of constraint in mammalian genomic sequence. *Genome Res.* 15, 901–913.
29. Ng, P.C., and Henikoff, S. (2003). SIFT: Predicting amino acid changes that affect protein function. *Nucleic Acids Res.* 31, 3812–3814.
30. Adzhubei, I.A., Schmidt, S., Peshkin, L., Ramensky, V.E., Gerasimova, A., Bork, P., Kondrashov, A.S., and Sunyaev, S.R. (2010). A method and server for predicting damaging missense mutations. *Nat. Methods* 7, 248–249.
31. Hecht, M., Bromberg, Y., and Rost, B. (2015). Better prediction of functional effects for sequence variants. *BMC Genomics* 16 Suppl 8, S1.
32. Gray, V.E., Hause, R.J., Luebeck, J., Shendure, J., and Fowler, D.M. (2018). Quantitative Missense Variant Effect Prediction Using Large-Scale Mutagenesis Data. *Cell Syst* 6, 116-124.e3.
33. Richards, S., Aziz, N., Bale, S., Bick, D., Das, S., Gastier-Foster, J., Grody, W.W., Hegde, M., Lyon, E., Spector, E., et al. (2015). Standards and guidelines for the interpretation of sequence variants: a joint consensus recommendation of the American College of Medical Genetics and Genomics and the Association for Molecular Pathology. *Genet. Med.* 17, 405–424.
34. Anders, S., Pyl, P.T., and Huber, W. (2015). HTSeq—a Python framework to work with high-throughput sequencing data. *Bioinformatics* 31, 166–169.
35. Anders, S., and Huber, W. (2010). Differential expression analysis for sequence count data. *Genome Biol.* 11, R106.
36. Benjamini, Y Controlling the False Discovery Rate: A Practical and Powerful Approach to Multiple Testing.
37. Mathys, H., Basquin, J., Ozgur, S., Czarnocki-Cieciura, M., Bonneau, F., Aartse, A., Dziembowski, A., Nowotny, M., Conti, E., and Filipowicz, W. (2014). Structural and biochemical insights to the role of the CCR4-NOT complex and DDX6 ATPase in microRNA repression. *Mol. Cell* 54, 751–765.

38. Pettersen, E.F., Goddard, T.D., Huang, C.C., Couch, G.S., Greenblatt, D.M., Meng, E.C., and Ferrin, T.E. (2004). UCSF Chimera--a visualization system for exploratory research and analysis. *J Comput Chem* **25**, 1605–1612.
39. de Chaumont, F., Dallongeville, S., Chenouard, N., Hervé, N., Pop, S., Provoost, T., Meas-Yedid, V., Pankajakshan, P., Lecomte, T., Le Montagner, Y., et al. (2012). Icy: an open bioimage informatics platform for extended reproducible research. *Nat. Methods* **9**, 690–696.
40. Ernoult-Lange, M., Baconnais, S., Harper, M., Minshall, N., Souquere, S., Boudier, T., Bénard, M., Andrey, P., Pierron, G., Kress, M., et al. (2012). Multiple binding of repressed mRNAs by the P-body protein Rck/p54. *RNA* **18**, 1702–1715.
41. Kamenska, A., Simpson, C., Vindry, C., Broomhead, H., Bénard, M., Ernoult-Lange, M., Lee, B.P., Harries, L.W., Weil, D., and Standart, N. (2016). The DDX6-4E-T interaction mediates translational repression and P-body assembly. *Nucleic Acids Res.* **44**, 6318–6334.
42. Tritschler, F., Eulalio, A., Helms, S., Schmidt, S., Coles, M., Weichenrieder, O., Izaurralde, E., and Truffault, V. (2008). Similar modes of interaction enable Trailer Hitch and EDC3 to associate with DCP1 and Me31B in distinct protein complexes. *Mol. Cell. Biol.* **28**, 6695–6708.
43. Sharif, H., Ozgur, S., Sharma, K., Basquin, C., Urlaub, H., and Conti, E. (2013). Structural analysis of the yeast Dhh1-Pat1 complex reveals how Dhh1 engages Pat1, Edc3 and RNA in mutually exclusive interactions. *Nucleic Acids Res.* **41**, 8377–8390.
44. Huang, D.W., Sherman, B.T., Tan, Q., Kir, J., Liu, D., Bryant, D., Guo, Y., Stephens, R., Baseler, M.W., Lane, H.C., et al. (2007). DAVID Bioinformatics Resources: expanded annotation database and novel algorithms to better extract biology from large gene lists. *Nucleic Acids Res.* **35**, W169-175.
45. Courel, M., Clement, Y., Foretek, D., Vidal, O., Yi, Z., Kress, M., Vindry, C., Benard, M., Bossevain, C., Antoniewski, C., et al. (2018). GC content shapes mRNA decay and storage in human cells. *BioRxiv*.
46. Thoreen, C.C., Chantranupong, L., Keys, H.R., Wang, T., Gray, N.S., and Sabatini, D.M. (2012). A unifying model for mTORC1-mediated regulation of mRNA translation. *Nature* **485**, 109–113.
47. Costa-Mattioli, M., and Monteggia, L.M. (2013). mTOR complexes in neurodevelopmental and neuropsychiatric disorders. *Nat. Neurosci.* **16**, 1537–1543.
48. Sengoku, T., Nureki, O., Nakamura, A., Kobayashi, S., and Yokoyama, S. (2006). Structural basis for RNA unwinding by the DEAD-box protein *Drosophila* Vasa. *Cell* **125**, 287–300.
49. Bifano, A.L., Turk, E.M., and Caprara, M.G. (2010). Structure-guided mutational analysis of a yeast DEAD-box protein involved in mitochondrial RNA splicing. *J. Mol. Biol.* **398**, 429–443.
50. Lessel, D., Schob, C., Küry, S., Reijnders, M.R.F., Harel, T., Eldomery, M.K., Coban-Akdemir, Z., Denecke, J., Edvardson, S., Colin, E., et al. (2017). De Novo Missense Mutations in DHX30 Impair Global Translation and Cause a Neurodevelopmental Disorder. *Am. J. Hum. Genet.* **101**, 716–724.
51. Snijders Blok, L., Madsen, E., Juusola, J., Gilissen, C., Baralle, D., Reijnders, M.R.F., Venselaar, H., Helsmoortel, C., Cho, M.T., Hoischen, A., et al. (2015). Mutations in DDX3X Are a Common Cause of

Unexplained Intellectual Disability with Gender-Specific Effects on Wnt Signaling. *Am. J. Hum. Genet.* 97, 343–352.

52. Wang, X., Posey, J.E., Rosenfeld, J.A., Bacino, C.A., Scaglia, F., Immken, L., Harris, J.M., Hickey, S.E., Mosher, T.M., Slavotinek, A., et al. (2018). Phenotypic expansion in DDX3X - a common cause of intellectual disability in females. *Ann Clin Transl Neurol* 5, 1277–1285.

53. Shamseldin, H.E., Rajab, A., Alhashem, A., Shaheen, R., Al-Shidi, T., Alamro, R., Al Harassi, S., and Alkuraya, F.S. (2013). Mutations in DDX59 implicate RNA helicase in the pathogenesis of orofacioidigital syndrome. *Am. J. Hum. Genet.* 93, 555–560.

54. Salpietro, V., Efthymiou, S., Manole, A., Maurya, B., Wiethoff, S., Ashokkumar, B., Cutrupi, M.C., Dipasquale, V., Manti, S., Botia, J.A., et al. (2018). A loss-of-function homozygous mutation in DDX59 implicates a conserved DEAD-box RNA helicase in nervous system development and function. *Hum. Mutat.* 39, 187–192.

55. Faily, S., Perveen, R., Urquhart, J., Chandler, K., and Clayton-Smith, J. (2017). Confirmation that mutations in DDX59 cause an autosomal recessive form of oral-facial-digital syndrome: Further delineation of the DDX59 phenotype in two new families. *Eur J Med Genet* 60, 527–532.

56. Telley, L., Govindan, S., Prados, J., Stevant, I., Nef, S., Dermitzakis, E., Dayer, A., and Jabaudon, D. (2016). Sequential transcriptional waves direct the differentiation of newborn neurons in the mouse neocortex. *Science* 351, 1443–1446.

57. Nicklas, S., Okawa, S., Hillje, A.-L., González-Cano, L., Del Sol, A., and Schwamborn, J.C. (2015). The RNA helicase DDX6 regulates cell-fate specification in neural stem cells via miRNAs. *Nucleic Acids Res.* 43, 2638–2654.

58. Quartier, A., Chatrousse, L., Redin, C., Keime, C., Haumesser, N., Maglott-Roth, A., Brino, L., Le Gras, S., Benchoua, A., Mandel, J.-L., et al. (2018). Genes and Pathways Regulated by Androgens in Human Neural Cells, Potential Candidates for the Male Excess in Autism Spectrum Disorder. *Biol. Psychiatry*.

59. Lennox, A.L., Jiang, R., Suit, L., Fregeau, B., Sheehan, C.J., Aldinger, K.A., Moey, C., Lobach, I., Mirzaa, G., Afenjar, A., et al. (2018). Pathogenic *DDX3X* mutations impair RNA metabolism and neurogenesis during fetal cortical development. *BioRxiv*.

60. Cougot, N., Bhattacharyya, S.N., Tapia-Arancibia, L., Bordonné, R., Filipowicz, W., Bertrand, E., and Rage, F. (2008). Dendrites of mammalian neurons contain specialized P-body-like structures that respond to neuronal activation. *J. Neurosci.* 28, 13793–13804.

61. Zeitelhofer, M., Karra, D., Macchi, P., Tolino, M., Thomas, S., Schwarz, M., Kiebler, M., and Dahm, R. (2008). Dynamic interaction between P-bodies and transport ribonucleoprotein particles in dendrites of mature hippocampal neurons. *J. Neurosci.* 28, 7555–7562.

62. Kiebler, M.A., and Bassell, G.J. (2006). Neuronal RNA granules: movers and makers. *Neuron* 51, 685–690.

63. Miller, L.C., Blandford, V., McAdam, R., Sanchez-Carbente, M.R., Badeaux, F., DesGroseillers, L., and Sossin, W.S. (2009). Combinations of DEAD box proteins distinguish distinct types of RNA: protein complexes in neurons. *Mol. Cell. Neurosci.* 40, 485–495.

64. Lennox, A.L., Mao, H., and Silver, D.L. (2018). RNA on the brain: emerging layers of post-transcriptional regulation in cerebral cortex development. *Wiley Interdiscip Rev Dev Biol* 7,.

FIGURE TITLES AND LEGENDS:

Figure 1. Individuals with intellectual disability and developmental delay and rare *de novo* missense variants in *DDX6*. Pictures of individuals with rare *de novo* missense variants in *DDX6* (Subjects S1, S2, S4, and S5).

Figure 2. Localization of the different *de novo* missense variants in *DDX6*

(A) Linear representation of the *DDX6* protein (NP_004388) with highlighted functional DExD/H-box motifs. *De novo* missense variants identified in individuals with ID are indicated by red dashed lines, and missense variants observed in the gnomAD population are plotted in orange with an indication of the number of individuals carrying them. Motif residue numbers and colors are as follows: motifs Q (115-123) and GG (201-203) in yellow; motifs I (140-146) and II (DEAD) (246-249) in dark green; motifs Ia (171-181) and Ib (222-225) in orange, motif IV (338-340) and V (395-399) in light green; and motifs III (277-279), QxxR (370-373), and VI (419-427) in grey. Motifs Q, I, II, V and VI are involved in ATP binding and motifs GG, QxxR, Ia, Ib, IV and V are involved in RNA binding. Motif III is involved in intramolecular interactions¹³. **(B)** Heatmap spanning the linear *DDX6* protein representing *in silico* impact (effect) predictions of all possible amino acid substitution mutations in *DDX6* from the SNAP2 classifier. Dark red indicates a strong signal for effect, white indicates weak signals, and blue a strong signal for

neutral/no effects. **(C)** Mapping of missense variants identified in gnomAD population (blue spheres) and in probands (red spheres) on a 3-D representative structure of DDX6 in complex with the CNOT1 MIF4G (pink) domain and 4E-T CHD (green) domain (PDB ID: 5ANR). The two RecA-like units of DDX6 are colored in grey (helicase ATP-binding domain) and yellow (helicase C-terminal domain). **(D)** Hydrophobicity surface model of DDX6 (PDB ID: 4CT5) using Chimera. Kyte-Doolittle scale coloring was used with colors ranging from dodger blue for the most hydrophilic, to white at neutral, to orange red for the most hydrophobic regions. Missense variants identified in probands have been highlighted in yellow.

Figure 3. Fibroblasts from individuals S1 and S2 contain a low number of PBs

(A) Fibroblasts from an unrelated, age-matched control individual and from S2 carrying the DDX6-p.Cys390Arg variant were immunostained with DDX6 and EDC4 antibodies. Nuclei were stained with DAPI. Arrows point to some selected PBs within cells. Scale bar = 20 μ m. **(B)** Fibroblasts from S1 carrying the DDX6-p.Arg373Gln variant and her healthy parents were analyzed as in (A) except that cells were grown 2h at 30°C before fixation. Scale bar = 20 μ m. **(C)** Quantification of fibroblasts having PBs. PB-containing cells were counted and plotted as a percentage of total cells (98 to 126 cells from 3 and 4 independent experiments for S2 and S1, respectively). Error bars, SD; t-test: $p < 0.0001$ for both probands, as compared with their respective control.

Figure 4. Rare missense variants in DDX6 affect its interaction with protein partners and PB formation

(A-C) Mutated DDX6 proteins are defective for PB assembly. **(A)** Complementation assays. HeLa cells were depleted for endogenous *DDX6* by transfection of a siRNA targeting *DDX6* 3'UTR at the time of plating (control). After 24 h, cells were transfected or not with indicated FLAG-DDX6-HA plasmids. 40 h later, cells were analyzed by immunofluorescence using indicated antibodies. Scale bar = 10 μ m. **(B)** Protein extracts from cells transfected or not with siRNA were analyzed by western blot with indicated antibodies to verify the DDX6 depletion. The DDX6 signal, normalized using the ribosomal protein S6, is indicated below. **(C)** The number of PBs per cell was counted in 3 independent experiments (21-67 cells per experiment) and expressed as the relative percentage of PBs compared to the complementation with wild-type DDX6. FLAG-DDX6-p.Arg373Gln, -p.Cys390Arg, -p.Thr391Ile, and -p.Thr391Pro correspond to the DDX6 variants identified in Subjects 1, 2, 3 and 4, respectively. Error bars, SD; t-test: $p < 0.0001$ for all mutants, as compared to wild-type. **(D)** DDX6 pathogenic variants impair ligand binding. HEK293 cells were depleted for endogenous DDX6 and transfected 24 h later with indicated FLAG-DDX6-HA plasmids as in (A-C). 48 h later, proteins were extracted in the presence of RNaseA and immunoprecipitated with anti-FLAG M2 antibodies. 10% of the eluates were analyzed by western blot using the same antibody (bottom frame), while bound proteins were revealed from the remaining eluates by western blotting with indicated antibodies (upper frame). Input corresponds to 30 μ g of HEK293 proteins. Indicated under the panels are the percentages of binding proteins compared to immunoprecipitation with the wild-type DDX6, after normalization using the amount of each immunoprecipitated FLAG protein. Similar results were obtained in 3 to 6 independent immunoprecipitation experiments.

Figure 5. DDX6 targets and mRNA-encoding proteins involved in translation initiation are enriched among genes upregulated in individual S2.

(A) Biotype distribution (according to Ensembl) of the differentially-expressed (DE) genes identified in S2. (B) Pathway enrichment analysis revealed a significant enrichment of GO terms Biological Process and Molecular Function related to protein translation, ribosome and RNA processing, and of KEGG pathway “ribosome” among the upregulated genes. (C) The mRNAs up (orange boxes) and down-regulated (green boxes) in Subject 2 (S2) were analyzed for their enrichment in a DDX6 CLIP experiment (left panel) and their differential expression after DDX6 silencing (right panel), both in K562 cells. The analysis was performed using various p-value thresholds for the differential expression in S2, as indicated. The distribution of the whole dataset (all) is given for comparison (grey boxes). The whiskers indicate the 10-90 percentiles. Up-regulated mRNAs in S2 are preferential DDX6 targets and preferentially up-regulated after DDX6 depletion in an erythroid cell line. (D) Up-regulated mRNAs in S2 tend to be excluded from PBs. The mRNAs up and down-regulated in S2 were analyzed for their enrichment in purified PBs, as in (C). (E) Up-regulated mRNA in S2 tend to have a high GC content. In panels C to E, two-tail Mann-Whitney tests were performed with respect to all mRNAs: ***, $p < 0.0005$; **, $p < 0.005$.

Table 1. Pathogenic *DDX6* variants in individuals with ID.

Table 2. Clinical features of individuals with *de novo* pathogenic variants in *DDX6*.

Table 1. Pathogenic *DDX6* variants in individuals with ID

Coordinate (HG19/GRCh37)	Variant (NM_004397.5)	Exon	Inheritance	Present in gnomAD database?	CADD	GERP++ RS Score (Vertebrates)	Envision Score	PolyPhen (HumVar)	SIFT	<i>DDX6</i> O-E / pLI (gnomAD)	<i>DDX6</i> Missense Z-Score (gnomAD)	ACMG Classification	Individuals
Chr11: 118627025:C:T	c.1118G>A p.Arg373Gln	11	<i>de novo</i>	no	31	19.02	0.51 (3%-ile)	1.0 (probably damaging)	0.0 (deleterious)			Likely pathogenic (PS2,PM2,PP3)	S1
Chr11: 118626975:A:G	c.1168T>C p.Cys390Arg	11	<i>de novo</i>	no	32	19.02	0.42 (<1%-ile)	1.0 (probably damaging)	0.0 (deleterious)			Likely pathogenic (PS2,PM2,PP3)	S2
Chr11: 118626971:G:A	c.1172C>T p.Thr391Ile	11	<i>de novo</i>	no	34	19.02	0.65 (21%-ile)	0.973 (probably damaging)	0.01 (deleterious)	0.04 / 1.0	3.93	Likely pathogenic (PS2,PM2,PP3)	S3
Chr11: 118626972:T:G	c.1171A>C p.Thr391Pro	11	<i>de novo</i>	no	27.6	19.02	0.68 (26%-ile)	0.963 (probably damaging)	0.02 (deleterious)			Likely pathogenic (PS2,PM2,PP3)	S4
Chr11: 118627028:T:C	c.1115A>G p.His372Arg	11	<i>de novo</i>	no	25.6	17.86	0.90 (71%-ile)	0.376 (benign)	0.03 (deleterious)			Likely pathogenic (PS2,PM2)	S5

Footnote: Envision: 0% (most damaging) – 100% (most wild-type-like).

Table 2. Clinical features of individuals with *de novo* pathogenic variants in *DDX6*

	Subject 1	Subject 2	Subject 4	Subject 5
Sex / Age at last exam	Female / 5 yrs	Male, 6 yrs	Male / 10 yrs	Female / 13 yrs
<i>DDX6</i> Variant (NIM_004397.5)	c.1118G>A (p.Arg373Gln)	c.1168T>C (p.Cys390Arg)	c.1171A>C (p.Thr391Pro)	c.1115A>G p.(His372Arg)
Inheritance	<i>de novo</i>	<i>de novo</i>	<i>de novo</i>	<i>de novo</i>
Intellectual disability	+	+	+	+
Developmental delay	+	+	+	+
Speech delay	+ (nonverbal)	+	+	+
Small head circumference (<2SD)	+	+	-	-
MRI brain anomalies	hypoplastic posterior corpus callosum (27mo)	-	-	wide liquor spaces, thin corpus callosum, mild delay of myelination
Seizures	-	-	h/o staring spell, normal EEG	-
Hypotonia	mild, axial	+	-	+
Gait	walked w/ support till 27m, many falls from balance issues	-	instability/ delayed coordination, toe-walking	trouble with walking, using wheelchair for longer distances
Digit abnormalities / arthrogryposis	overriding second toes bilaterally	syndactyly II-III of the feet	tapered fingers, hypermobile flat feet	tapered fingers, overriding toes
Facial dysmorphism	hypertelorism, small palpebral fissures, bilateral epicanthus, arched eyebrows	hypertelorism, small palpebral fissures, bilateral epicanthus	arched eyebrows	high bossing forehead, bitemporal narrowness, telecanthus, epicanthus
Eyes	strabismus, hypermetropia	strabismus, hypermetropia	slight anisocoria	strabismus; hypermetropia
Ears	low set, petite and rotated. overfolded superior pinna	low set	-	overfolded upper helix
Mouth	high arched palate, smooth prominent philtrum	-	-	-
Heart abnormalities	patent foramen ovale, aberrant rt subclavian artery, cardiac murmur	atrial septal defect with spontaneous closing	<i>no imaging</i>	patent foramen ovale
Congenital hydronephrosis / vesicoureteral reflux	+	-	-	-
Feeding difficulties / GERD	+ (G-tube)	+	h/o abdominal pain/ constipation, unexplained elevated LFTs-resolved	+

Genitourinary anomalies	anteriorly placed anus, normal genitalia	cryptorchidism	micropenis	-
Other	recurrent infections, oligohydramnios, malrotated right pelvic kidney	supernumerary nipple, inguinal hernia	hyposmia/ anosmia, femoral retroversion, external tibial torsion, progressive striae on legs, photosensitivity with severe eczematous rash on hands, advanced bone age, mild truncal obesity, anxiety, motor stereotypies	single umbilical artery, delayed closure of fontanel, mild hip dysplasia, pes plano valgus, mild obesity, scoliosis



S1



S2

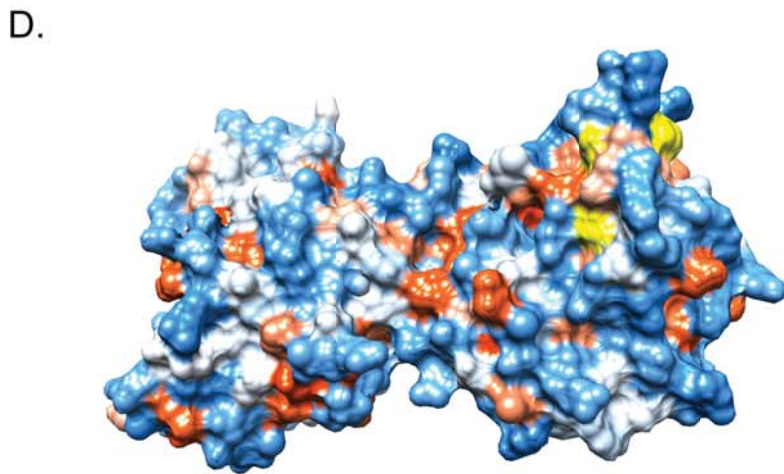
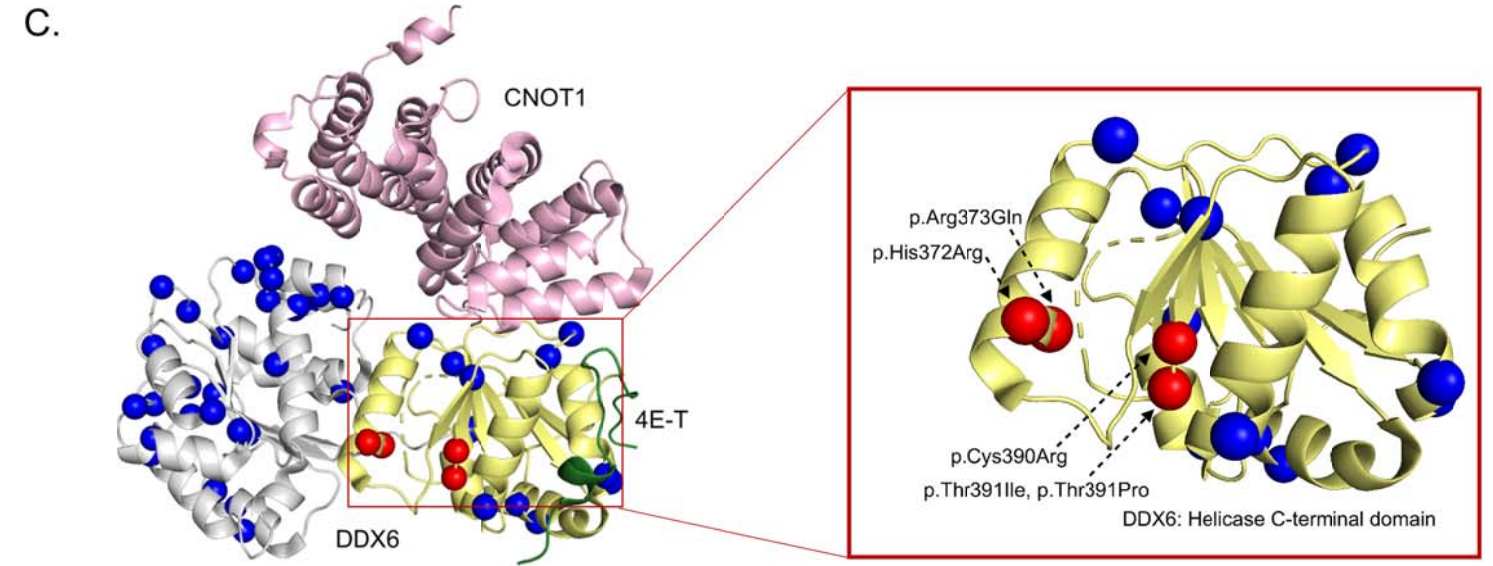
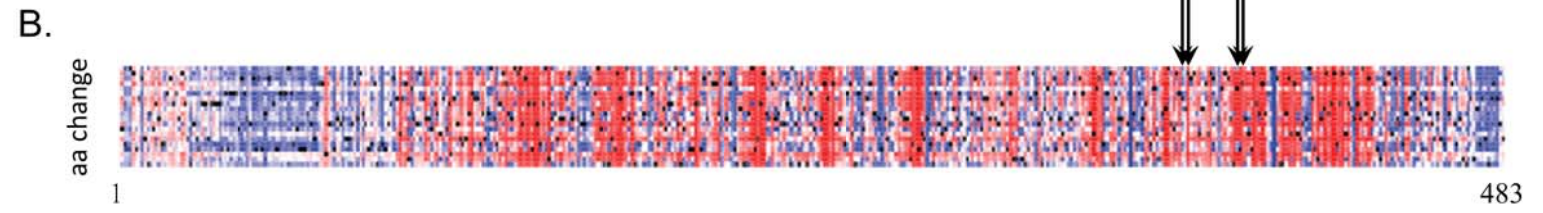
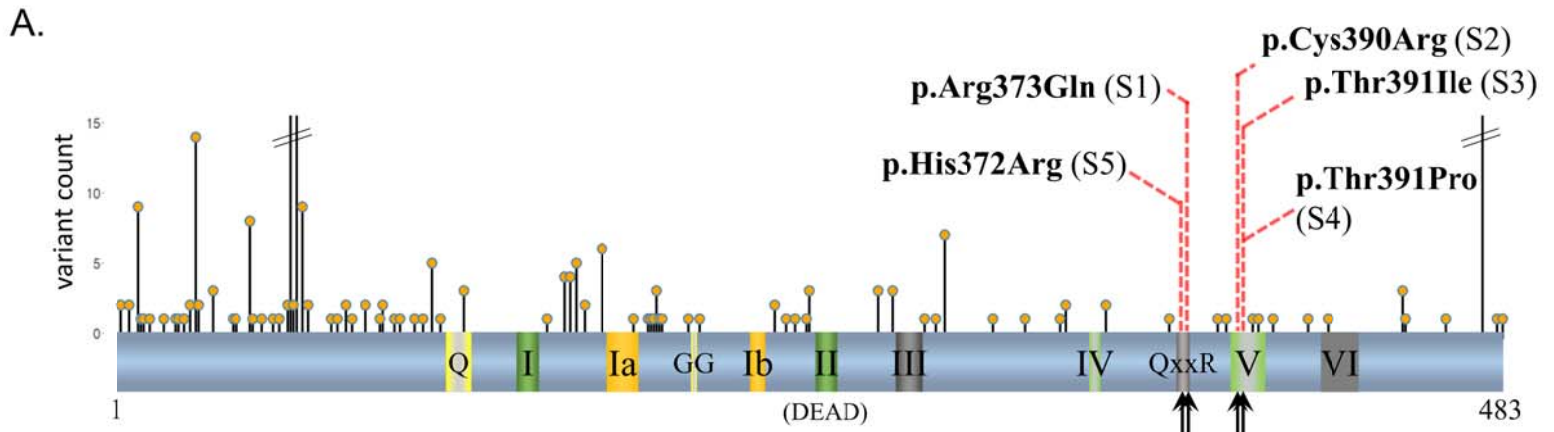


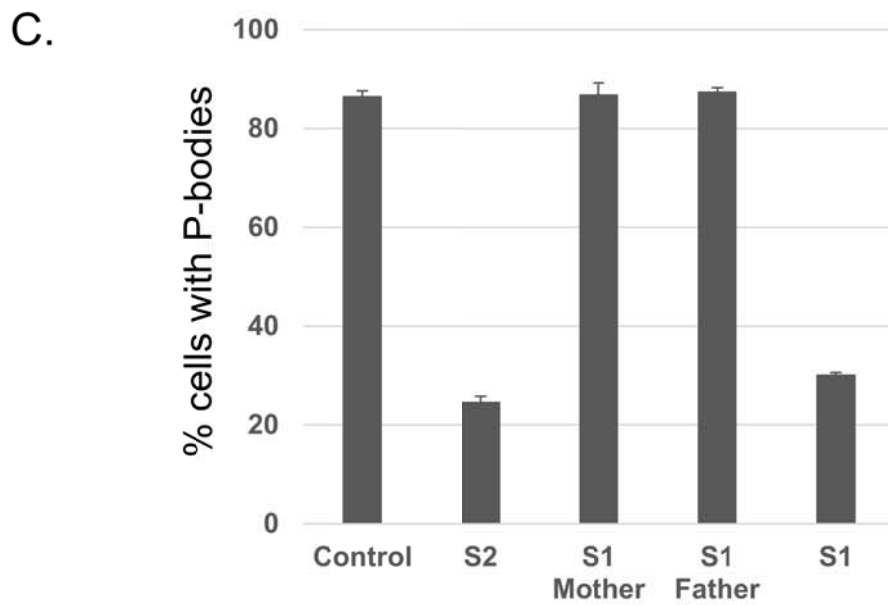
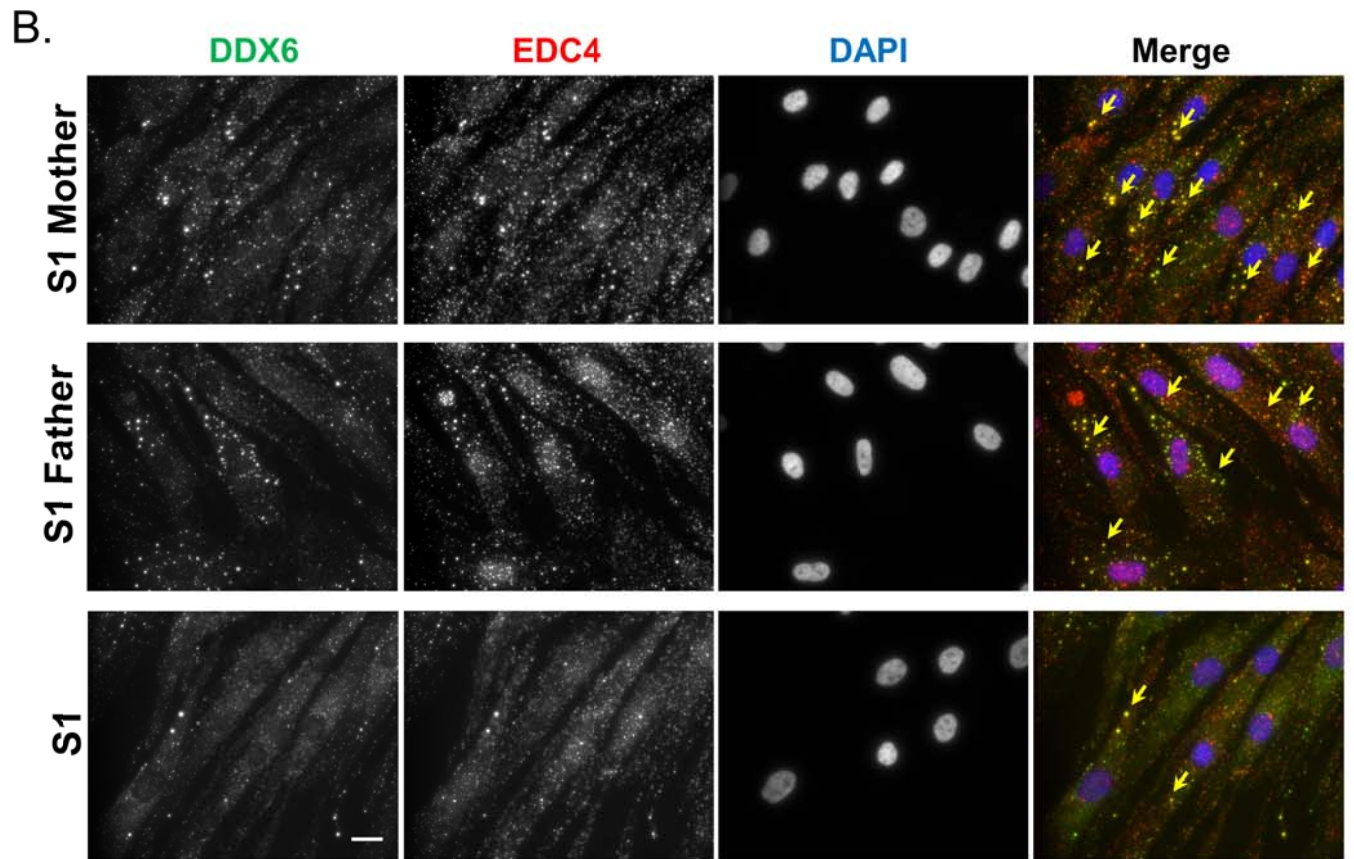
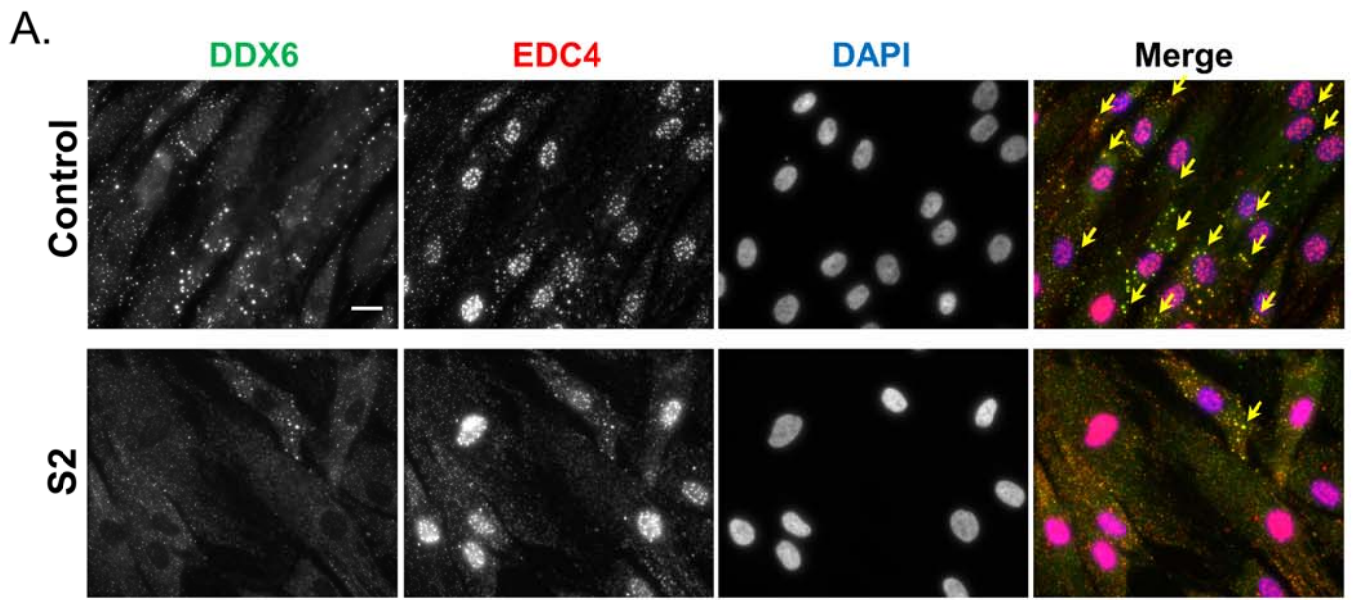
S4



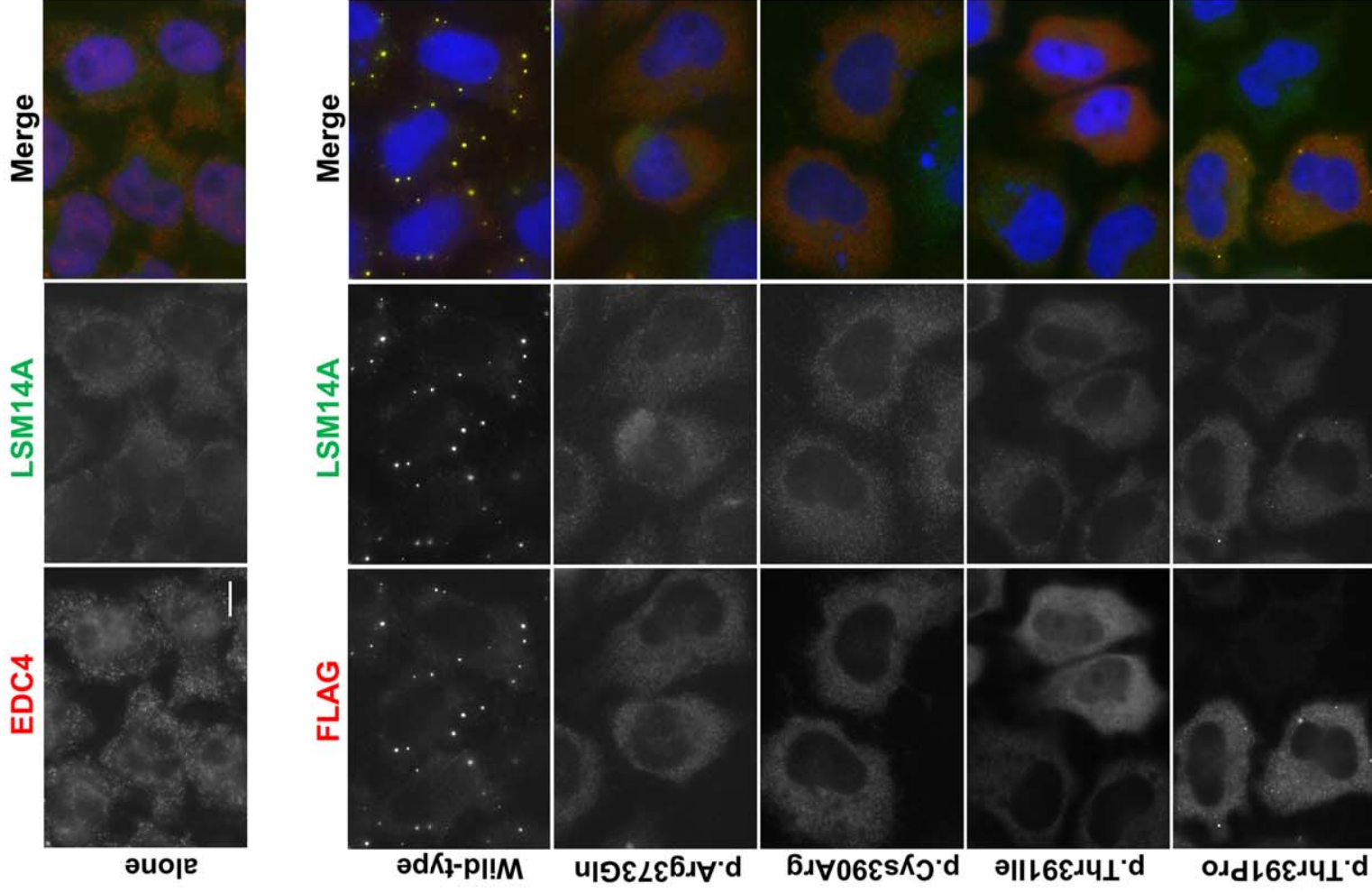
S5



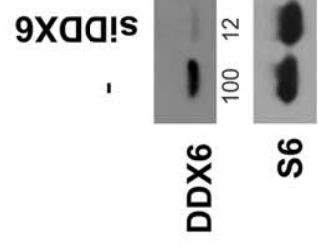




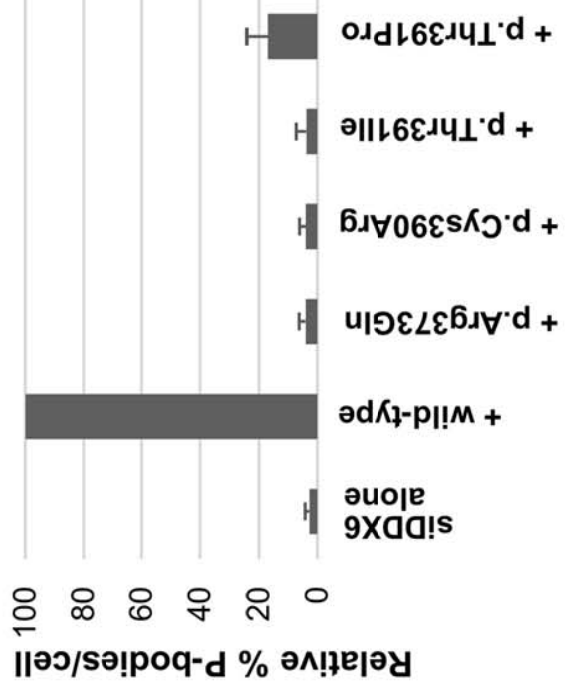
A.



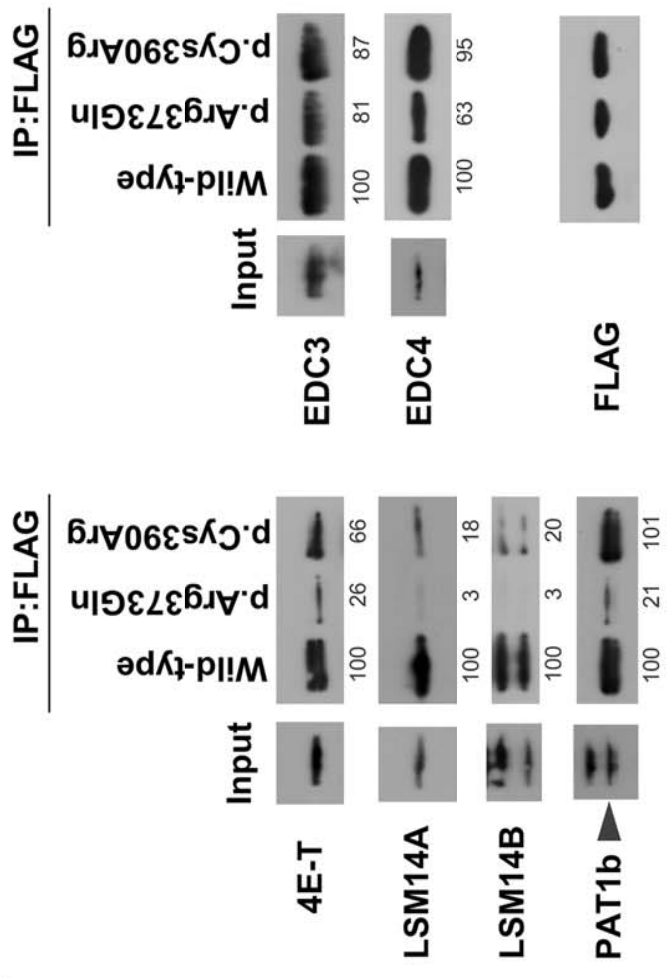
B.



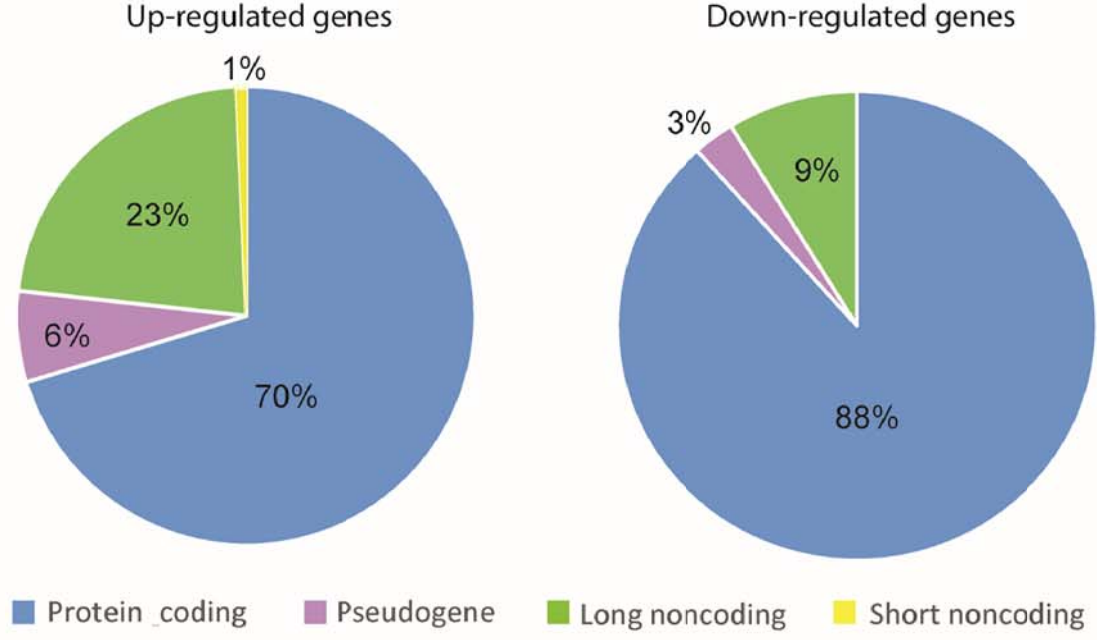
C.



D.



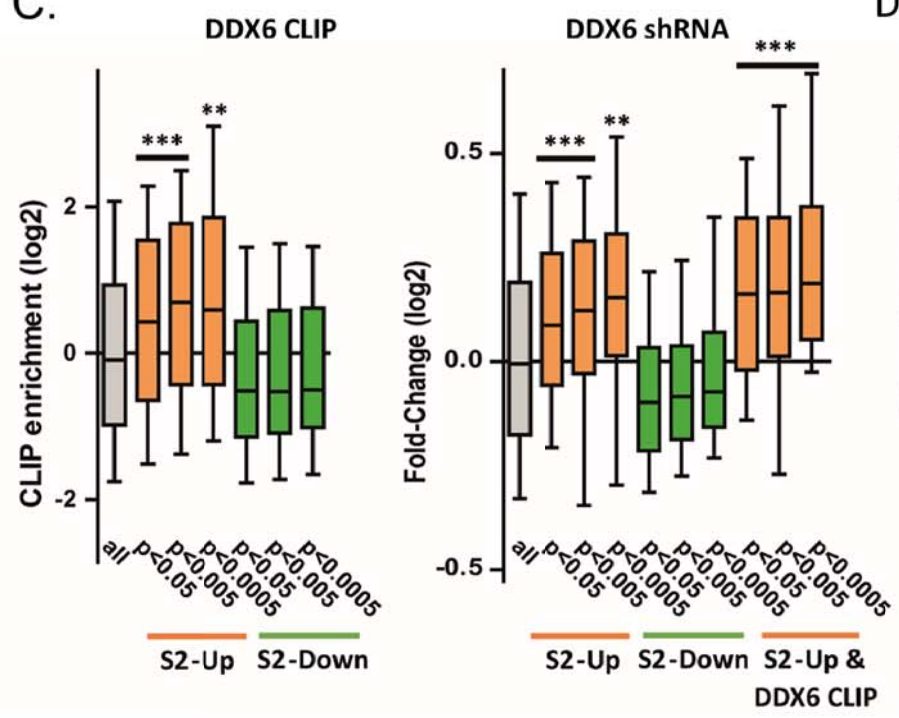
A.



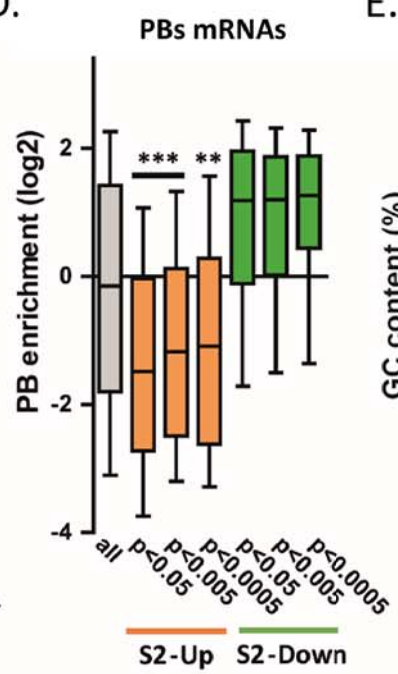
B.

Pathways enrichment	Fold Enrichment (number of genes)	Pvalue	Adj pvalue
GOTERM_BP_DIRECT			
SRP-dependent cotranslational membrane targeting (GO:0006614)	12.5 (27)	2.5e-21	2.0e-18
formation of translation preinitiation complex (GO:0001731)	11.3 (6)	1.5e-04	3.3e-02
viral transcription (GO:0019083)	10.5 (27)	3.1e-19	1.7e-16
cytoplasmic translation (GO:0002181)	10.4 (6)	2.2e-04	4.3e-02
translational initiation (GO:0006413)	10.2 (32)	2.4e-22	3.8e-19
mRNA degradation, nonsense-mediated decay (GO:0000184)	9.9 (27)	1.6e-18	6.3e-16
rRNA processing (GO:0006364)	6.1 (30)	1.2e-14	3.9e-12
translation (GO:0006412)	4.8 (28)	3.2e-11	8.5e-09
GOTERM_MF_DIRECT			
structural constituent of ribosome (GO:0003735)	5.4 (28)	2.5e-12	1.5e-09
poly(A) RNA binding (GO:0003723)	1.9 (51)	1.1e-05	3.1e-03
KEGG_PATHWAY			
Ribosome (map03010)	7.9 (28)	3.3e-17	7.2e-15

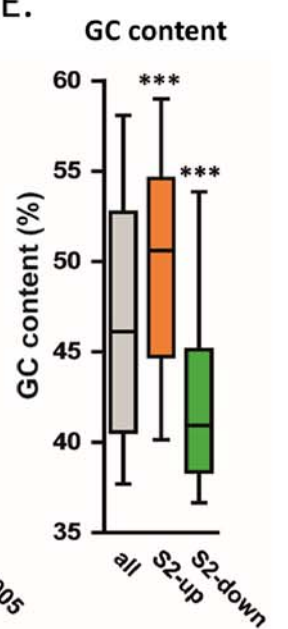
C.



D.



E.



Supplemental Note: Case Reports

Subject 1

She is a 3-year old girl of non-consanguineous parents with Hungarian/Puerto Rican descent (mother) and Hispanic/Mexican descent (father). Regarding family history, mother was noted to have a half-brother diagnosed with autism. She presented to TGen's Center for Rare Childhood Disorders exhibiting several conditions including global developmental delay, microcephaly, dysmorphic features, bilateral vesicoureteral reflux with hydronephrosis, and hypoplasia of the posterior corpus callosum. Pregnancy was uneventful up until the discovery of oligohydramnios at five months gestation. During this time, a fetal ultrasound revealed a low-lying kidney and renal reflux. Following 34 weeks of gestation, the patient was born via C-section with a birth weight of 4 pounds and 14 ounces. APGARs are not known. She was admitted to the neonatal intensive care unit to address feeding problems. During that time, she required nasogastric feedings and received oxygen by nasal cannula. After 3 weeks, the patient was discharged with bottle feedings. At 16 months, she underwent ureteral re-implantation surgery to correct the reflux. Neuroimaging studies were performed at 27 months of age. A brain MRI study revealed hypoplastic posterior corpus callosum. The CT scan of the brain appeared normal. Further diagnostic testing including karyotype, MECP2, fragile X, PWS methylation, CMA, and plasma acylcarnitine were performed with normal outcomes. Hearing tests conducted at that time were also normal. Developmental delays had been observed since birth without history of regression of developmental milestones. Rolling over was accomplished at 12 months and crawling at 16 months. At the time she was referred to the center, she was able to feed herself using both hands. She exhibited language delays, not yet communicating with words although she is able to vocalize and follow very simple commands. To overcome these delays, she participates in ST, PT, and OT and continues to make slow developmental progress. She is now able to walk independently, but requires assistance with dressing and toileting.

There is no history of seizures, pulmonary, ophthalmologic, and gastrointestinal problems. Physical observations were noted at her four year physical exam. The patient had a height of 101.8 cm (44%), weight of 15.6 kg (34%), and head circumference of 46.2 cm (2 SD below mean for age). Dysmorphic facial features included epicanthal folds, hypertelorism, and almond shaped eyes. Her ears were low set and posteriorly rotated with overfolded superior pinna. Furthermore, she had anteverted nares and a broad flat nasal root. Her hair was well grown for her age with two posterior hair whorls 2 cm apart. Her philtrum was prominent and she had a high arched palate. Her neurological examination revealed an alert, smiling, and interactive female. She responded to her name, vocalized, but did not use any words. Her face was symmetric and she made eye contact. A motor exam demonstrated mild axial hypotonia with normal strength and tone in upper and lower extremities. Deep tendon reflexes were present in upper and lower extremities. She was able to walk on her own and sit independently. She is noted to be quite socially outgoing.

Subject 2

He was born in 2011, first child of non-consanguineous parents with European descent. His father presented with bilateral clubfoot put in plaster in infancy. The mother had gestational diabetes during the pregnancy, treated by diet. The birth was accelerated due to alteration of the fetal cardiac rhythm and the patient presented transitory respiratory distress (APGARs were 4, 6, 10). At birth, the weight was 2650 g, the height 49 cm and the head circumference 33 cm. Hypotonia with sucking difficulties was noticed during the two first days of life. Abdominal and cerebral ultrasound, skeleton radiographs and otoacoustic emissions were normal. Echocardiography found atrial septal defect and patent foramen ovale. The patient also exhibited dysmorphic features with right plagiocephaly, small palpebral fissures, hypertelorism, bilateral epicanthus and asymmetric ears with overfolded superior pinna. He had a unilateral cryptorchidism, a syndactyly between the 2d and the 3th toes on right foot and a supernumerary nipple. The patient was operated of inguinal hernia in the first months of life. The growth was regular at -2.5 SD for the weight, -1 SD for the height and -2 SD for head circumference. Psychomotor retardation was noticed at 9 months old with a sit station delayed. Walk was acquired at 26 months and toilet training at 5 years.

The patient also exhibited language delay and comprehension and concentration troubles. He needed specialized education. He has no stereotypy or behavioral disorders but transitory sleep disturbance. Medical check-up was made for the weight retardation and did not find any medical trouble. Only masticatory troubles were highlighted. Ophthalmologic examination found strabismus (operated at 5 yo), canthi dystopia, hypermetropia and normal fundus. ENT evaluation found normal hearing but the patient did many ENT infections leading to tonsillectomy. Cerebral MRI found no cerebral malformation. CT scan showed craniostenosis of the metopic suture without chirurgical gesture necessary. Genetic testing including karyotype, array CGH, fragile X, high-throughput sequencing of 220 genes implicated in ID were performed with normal outcomes. At the last clinical examination at 6 years, the patient weighted 18 kg (-2.5SD) for 115 cm (-1 SD) and had a head circumference at 50 cm (-1.8 SD). He made simple sentences, wrote his name, fed himself, and bicycled (with 4 wheels). Pathologic excessive sociability was noticed.

Subject 4

This is an 11-year old boy of non-consanguineous parents of German and Irish descent. He was born at 36 3/7 weeks to a 28 year old G1P0->1 mother. Prenatal complications included gestational diabetes, infection (unknown type), and bleeding. He required resuscitation after a traumatic delivery and had hypoglycemia, but did not require a NICU stay. He was large for gestational age with a birth weight of 7 lbs 8 oz, birth length of 53.3 cm, and head circumference of 34.5 cm. He was seen by Ophthalmology at 2 months of age due to physiologic anisocoria and facial asymmetry. He was later seen by Orthopedics at 2.5 years of age due to concerns of toe-walking; diagnoses included femoral retroversion, external tibial torsion, and flat feet. He has a history of abdominal pain and constipation felt to be due to IBS, and at one point was found to have unexplained elevation of liver function tests. He has been noted to have autistic features, but does not meet criteria for a diagnosis of autism spectrum disorder. Other neurodevelopmental diagnoses include communication disorder, stereotypic movement disorder, motor coordination disorder, learning disorder, anxiety, and inattention. He had a full scale IQ of 70 using the Wechsler scale. Genetic tests including karyotype, microarray, and fragile X testing were all normal. He was evaluated by Endocrinology at 7 years of age due to concern about penile length, and possible anosmia/ hyposmia was noted. He had normal thyroid studies, growth hormone level, and bone age at that time, and was referred to Genetics and Urology for further evaluation. Of note, Urology did not feel that he has micropenis, but does have a buried penis and adhesions which should be re-evaluated at puberty. He was first seen by Genetics at 8 years of age and Kallmann syndrome was suspected, but a 13-gene testing panel was normal. Following this evaluation, there was concern for seizure activity due to a staring event and jerky movements in sleep, as well as persistent toe-walking and gait instability. An EEG, brain MRI, and lumbar spine MRI were normal. He was also seen extensively by Dermatology for dermatitis, juvenile spring eruption and allergic contact dermatitis. Biopsy of skin revealed spongiotic dermatitis. He was seen for follow-up in Genetics at 10 years of age, with new clinical features of mild truncal obesity, severe eczema of the hands, generalized sun sensitivity (erythema and pain after minimal exposure), and progressively worsening striae on thighs and lower legs. Urine porphyrins and whole exome sequencing were recommended. Urine porphyrins were normal. Whole exome sequencing revealed one variant of uncertain significance in *DDX6* (c.1171A>C), as well as a variant of uncertain significance in the *SLC16A2* gene (c.985G>A). Repeat thyroid studies including T4, T3 (free, total, and reverse) were normal, so we are less suspicious for the *SLC16A2* variant. He previously had a normal 24-hour free cortisol, but was re-evaluated by Endocrinology due to his striae. He had an elevated cortisol and ATCH, but it was later noted that this was following a course of high dose prednisone for his skin rash. Repeat ACTH was within normal limits; and cortisol was low. They recommended further evaluation to rule out iatrogenic adrenal insufficiency due to slight drop in growth velocity and history of treatment with prednisone. His bone age was advanced (2.9 SD above the mean); cortrosyn and growth hormone stimulation tests have not yet been completed.

Subject 5

She is the third child of non-consanguineous parents. She was born after an uncomplicated pregnancy and delivery at 41 weeks gestation. She was born with a single umbilical artery and a large slowly closing fontanel. There was prominent hypotonia, constipation, and feeding problems during the first years of her life. Her psychomotor development was severely delayed. On evaluation at age 1.5 years she had a high narrow prominent forehead, a large fontanel, strabismus, telecanthus, bilateral epicanthus, and a short nose with a broad tip and anteverted nares. She spoke her first words after the age of 3 years and was able to walk without support after the age of 5 years. She still has trouble walking. She walks instable like a young child, falls easily and cannot walk long distances. During recent years she also developed a scoliosis. She has no seizure and normal hearing. She attends a special school for children with severe learning problems. An ophthalmological evaluation showed prominent hypermetropia and right sided amblyopia. She further had mild bilateral hip dysplasia and an echocardiogram, performed because of a heart murmur, showed a patent foramen ovale. Renal ultrasound was normal, and a brain MRI showed non-specific abnormalities, including wide central and peripheral liquor spaces, a thin corpus callosum and a mildly delayed myelination. At age 11 years, her height was 149 cm (-0.11 SD), her weight 53 kg (+2.19 SD; weight for height) and her occipital head circumference was 52 cm (-0.76 SD). She had a narrow prominent forehead, deep set eyes, strabismus, epicanthic folds, broad nasal tip, short philtrum, and thin vermilion of the upper lip. She further had tapering fingers, overriding toes and pes plano valgus with joint hyperlaxity.

P26196	DDX6_H.sapiens	---QLGYSCFYIHAKMRQEHRNRVFDHF-RNGLCRNLVCTDLFTRGIDIQAVN	404
H9FQP5	DDX6_M.mulata	---QLGYSCFYIHAKMRQEHRNRVFDHF-RNGLCRNLVCTDLFTRGIDIQAVN	404
E2RR01	DDX6_Canis_lupus	---QLGYSCFYIHAKMRQEHRNRVFDHF-RNGLCRNLVCTDLFTRGIDIQAVN	404
P54823	DDX6_M.musculus	---QLGYSCFYIHAKMRQEHRNRVFDHF-RNGLCRNLVCTDLFTRGIDIQAVN	404
D3ZD73	DDX6_R.norvegicus	---QLGYSCFYIHAKMRQEHRNRVFDHF-RNGLCRNLVCTDLFTRGIDIQAVN	404
Q5ZKB9	DDX6_G.gallus	---QLGYSCFYIHAKMRQEHRNRVFDHF-RNGLCRNLVCTDLFTRGIDIQAVN	404
E7FD91	DDX6_X.laevis	---QLGYSCFYIHAKMRQEHRNRVFDHF-RNGLCRNLVCTDLFTRGIDIQAVN	405
P54824	DDX6_Danio_erio	---QLGYSCFYIHAKMRQEHRNRVFDHF-RNGLCRNLVCTDLFTRGIDIQAVN	403
P23128	DDX6_D.melanogaster	---ELGYCCYYIHAKMAQAHRNRVFDHF-RQGLCRNLVCSDLFTRGIDVQAVN	365
P39517	DHH1_S.cerevisiae	---DLGYSCYYSHARMKQQRNRKVFHEF-RQGVVRTLVCSDLLTRGIDIQAVN	353
Q92499	DDX1_HUMAN	-----DKKGHFVSCVCLHGDGRKPHERKQNLERF-KKGDVRFLLICTDVAARGIDIHGVP	585
P60842	IF4A1_HUMAN	-----ARDFTVSAMHGDMQKERDVMIMREF-RSGSSRVLIITDLLARGIDVQVVS	342
Q14240	IF4A2_HUMAN	-----ARDFTVSALHGDMDQKERDVMIMREF-RSGSSRVLIITDLLARGIDVQVVS	343
O00571	DDX3X_HUMAN	-----HEGYACTSIHGDRSQDRREALHQF-RSGKSPILVATAVAARGLDISNVK	511
Q9NQI0	DDX4_HUMAN	-----QEKISTTSIHGDMREQREEQALGDF-RFGKCPVLVATSVAAARGLDIENNVQ	610
P17844	DDX5_HUMAN	-----RDGWPAMGIHGDKSQERDQWVLEF-KHGKAPILITDVASRGLDVEDVK	411
P26196	DDX6_HUMAN	-----QLGYSCFYIHAKMRQEHRNRVFDHF-RNGLCRNLVCTDLFTRGIDIQAVN	404
Q13206	DDX10_HUMAN	-----LRPGVSILALHGRQQQMRMEVYNEF-VRKRAAVLFDIAARGLDFPAVN	385
Q9NUU7	DD19A_HUMAN	-----KEGHQVALLSGEMMVEQRAAVIERF-REGKEKVLVATNVCARGIDVEQVS	402
Q9UMR2	DD19B_HUMAN	-----KEGHQVALLSGEMMVEQRAAVIERF-REGKEKVLVATNVCARGIDVEQVS	403
Q9UHI6	DDX20_HUMAN	-----SKGFPAECISGNMNNQRLDAMAKL-KHFHCRVLIITDLTSTRGIDAIEKVN	379
Q9NR30	DDX21_HUMAN	-----IKQDAQSLHGDIPQQRREITLKGFRNGSFGVLVATNVAARGLDIPVD	507
Q9BUQ8	DDX23_HUMAN	-----SLEKMGYNACTLHGGKGOEQREFALSNI-KAGAKDILVATDVAGRGIDIQDVS	734
Q9GZR7	DDX24_HUMAN	-----LLKVLDIMPLTLHACMHQKQRLRNLEQF-ARLEDCVLLATDVAARGLDIPKVQ	657
Q9UHL0	DDX25_HUMAN	-----QDGHQVSLLSGELTVEQRASIIQRF-RDGKEKVLVATNVCARGIDVQVVT	408
Q96GQ7	DDX27_HUMAN	-----LLGLMGLQVGLHGNLSQTQRLLEALRRF-KDEQIDILVATDVAARGLDIEGVK	533
Q9NUL7	DDX28_HUMAN	-----ILDHDKIQHLRLQGMPALMRVGIQSF-QKSSRDILLCTDIASRGLDSTGVE	467
Q9H8H2	DDX31_HUMAN	ASGQ-LPSASMRLLKFLRLHGGMEQERTAVFQEF-SHSRRGVLLCTDVAARGLDLPQVT	598
O00148	DX39A_HUMAN	-----EQNFPAIAIHRGMAQERLSRYQQF-KDFQRRILVATNLFGRGMDIERVN	356
Q13838	DX39B_HUMAN	-----EQNFPAIAIHRGMAQERLSRYQQF-KDFQRRILVATNLFGRGMDIERVN	357
Q9UJV9	DDX41_HUMAN	-----LKGVEAVAIIHGKDKQERTKAIEAF-REGKKDVLVATDVASKGLDFPAIQ	502
Q86XP3	DDX42_HUMAN	-----QEGHNLGLLHGDMDQSERNKVISDF-KKKDIPVLVATDVAARGLDIPSIK	568
Q9NXZ2	DDX43_HUMAN	-----LGNISVESLHGDREQRREKALENF-KTGKVRILITDLASRGLDVHDTV	557
Q7L014	DDX46_HUMAN	-----RASYPMSLHGGIDQYDRDSIINDF-KNGTCKLLVATSVAAARGLDVKHLI	689
Q9H0S4	DDX47_HUMAN	-----LLRNLGFTAIPLHGQMSQSKRLGSLNKF-KAKARSILLATDVASRGLDIPHVD	333
P38919	IF4A3_HUMAN	-----EANFTVSSMHGDMPPQERESIMKEF-RSGASRVLIITDVWARGLDVPPQVS	347
Q9Y6V7	DDX49_HUMAN	-----MLRKFSFPTVALHSMKKQERFAALAKF-KSIIYRILITDVAARGLDIPVTQ	318
Q9BQ39	DDX50_HUMAN	-----IKQNAQCLHGDIAQSQREITLKGFRREGSFKVLVATNVAARGLDIPVD	458
Q8N8A6	DDX51_HUMAN	-----AFGGVDVAEFSSRYGPGQRMRILKQF-EQGKIQLLIATDATARGIDVQVVE	575
Q9Y2R4	DDX52_HUMAN	-----YEGINVDVIAERTQQRDNTVHSF-RAGKIWVLICTALLARGIDFKGVN	482
Q86TM3	DDX53_HUMAN	-----IQGISAESLHGSNEQSQDERAVEDF-KSGNIKILITDIVSRGLDLNDVT	537
Q8TDD1	DDX54_HUMAN	-----LLTTQRVSCAHIYALNDPTARKINLAKF-TLGKCTLIITDLAARGLDIPLLD	408
Q8NHQ9	DDX55_HUMAN	-----LVKGVKIMCIHGKMK-YKRNKIFMEF-RKLQSGILVCTDVMARGIDIPVNV	338
O95786	DDX58_HUMAN	KLSFLKPGILTGRGKNTQNTGMTLPQKCILDAFKASGDHNLITDVADEGIDIAQCN	710
Q5T1V6	DDX59_HUMAN	-----KITGLKSISIHSEKSIERKNILKGL-LEGDYEVVVATGVLGRGLDLISVR	515



Figure S1.

Conservation of DDX6 amino acid sequence among human DDX (DEAD-box) proteins and different species. The QxxR motif is highlighted in yellow and Motif V in light blue. Red lettering indicates the evolutionarily-conserved wild-type amino acid. White lettering indicates small, structurally-similar residues to Cysteine at position 390. Purple lettering at position 372 indicates glutamine or glutamate residues, or related/unreactive amino acids.

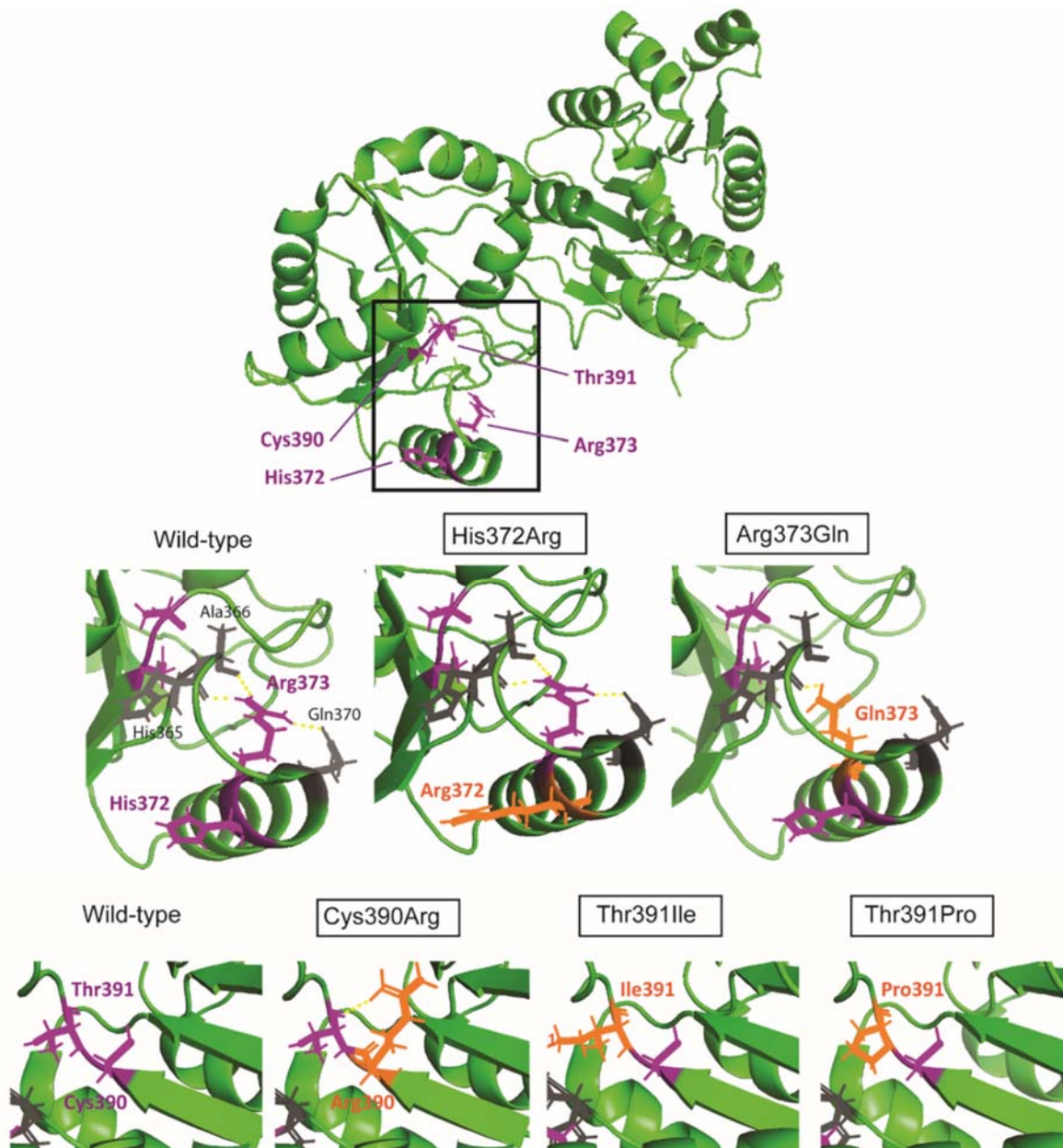


Figure S2.

3D structure of DDX6 with predicted bonding effects of the missense variants. DDX6 protein (open conformation, PDB: 4CT5) and amino acids changes of affected individuals were visualized using PyMol. In purple are the amino acids encoded by the reference sequence, in orange are the amino acids encoded by the DDX6 missense variants. Putative polar contacts (hydrogen bonds) between adjacent amino acids are represented by yellow dotted lines.

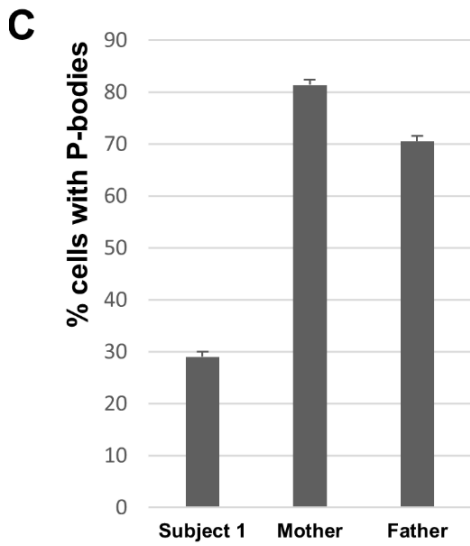
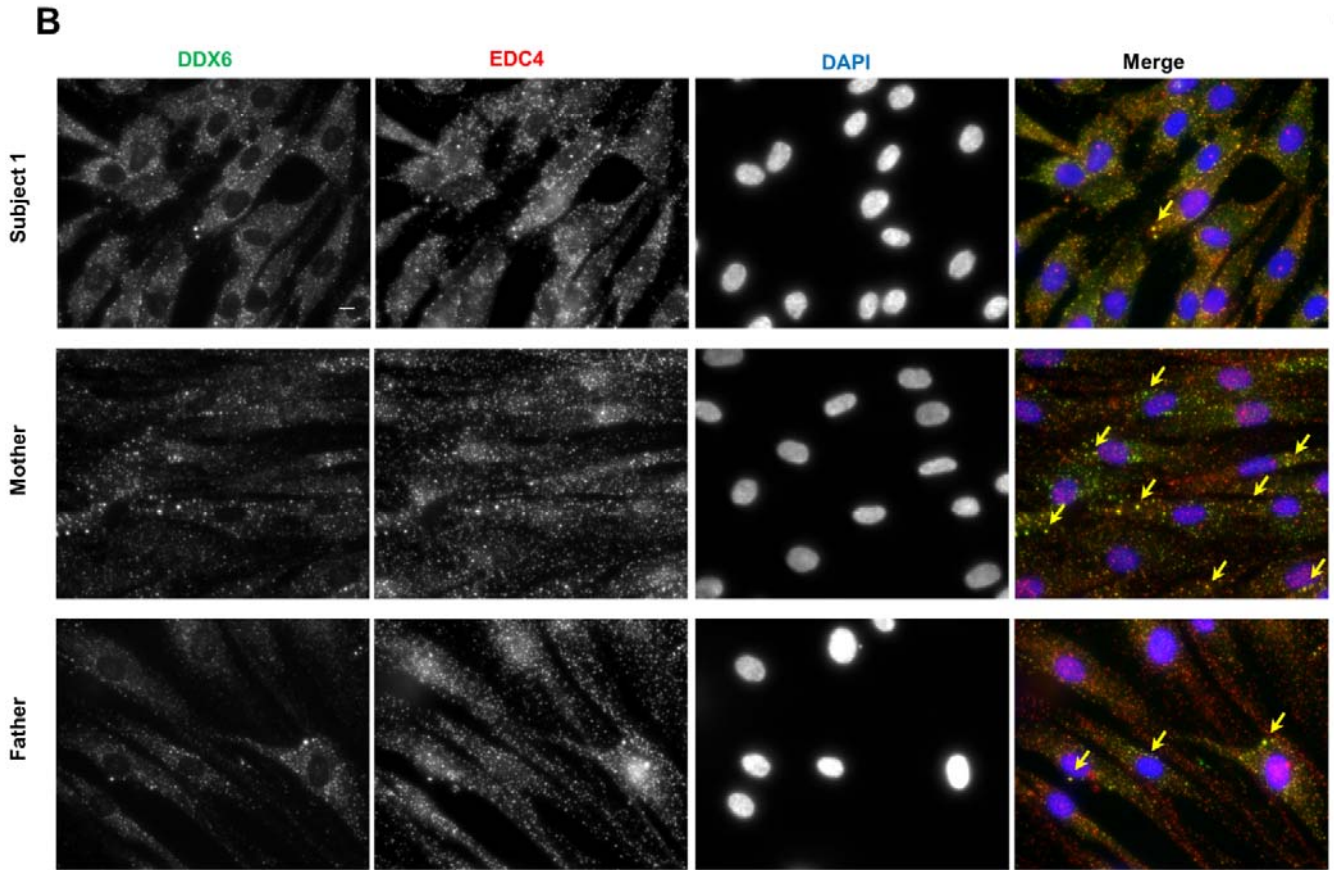
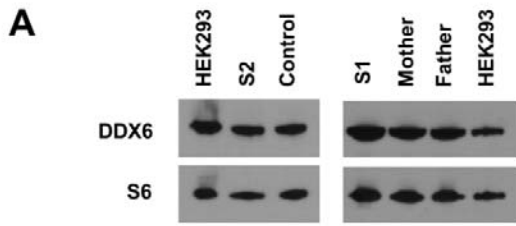


Figure S3.

DDX6 expression and PB formation in cells derived from affected individuals. (A)

Expression of DDX6 in fibroblasts from S1 and S2. 30 μ g of cytoplasmic protein extracts from HEK293 cells or fibroblasts from S2 and from a control individual were analyzed by western blotting with indicated antibodies. The DDX6 signal, normalized using the ribosomal protein S6, is indicated below. (B) Low PB formation in S1 fibroblasts; S1 nuclear family fibroblasts prior to 30°C treatment. Fibroblasts from S1 and her parents were grown at 37°C and immunostained with DDX6 and EDC4 antibodies. Nuclei were stained with DAPI. Arrows point to some selected PBs within cells. Bar = 20 μ m. (C) Quantification of fibroblasts having PBs. PB-containing cells were counted and plotted as a percentage of total cells (69 to 178 cells from 2 independent experiments). Error bars, SD; t-test: $p < 0.0001$ for proband, as compared with both controls.

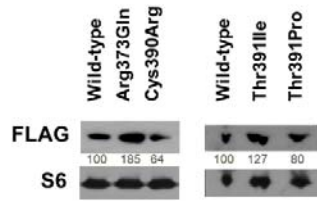
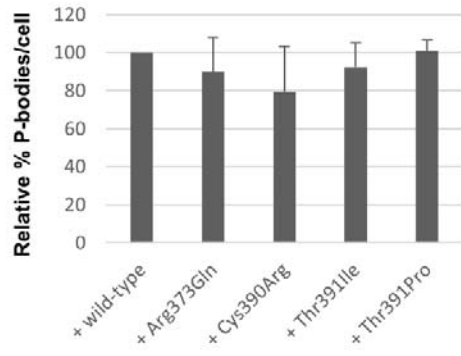
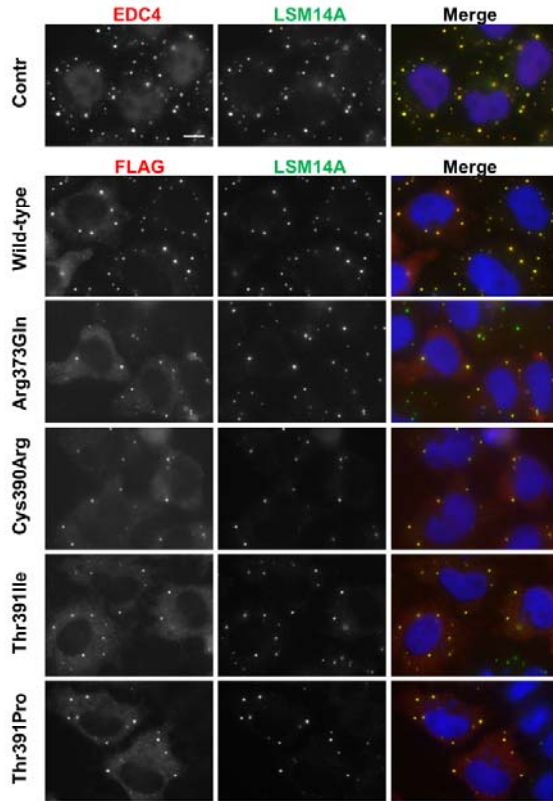
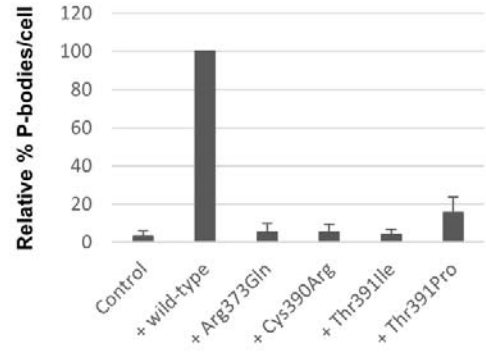
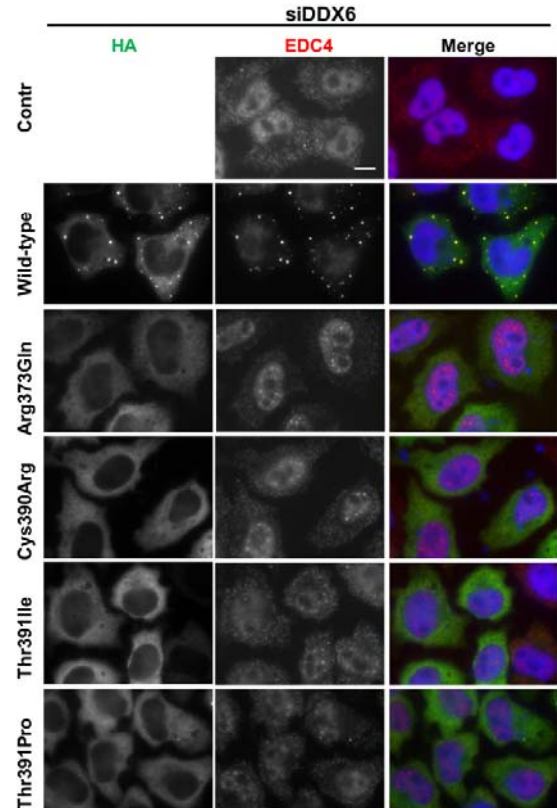
A**B****C**

Figure S4.

DDX6 containing the missense variants of affected individuals can be recruited in PBs but do not trigger PB assembly. (A) Expression of recombinant proteins. 30 μ g of cytoplasmic protein extracts from HeLa cells transfected with indicated FLAG-DDX6 plasmids named as in Figure 4 were analysed by western blotting with indicated antibodies. The FLAG signal, normalized using the ribosomal protein S6, is indicated below. (B) Localization of recombinant proteins. HeLa cells were transfected with FLAG-DDX6-HA plasmids as indicated and immunostained after 62 h with indicated antibodies. FLAG-DDX6-HA plasmids are named as in Figure 4. Bar = 10 μ m. Below is shown the number of PBs per cell counted in 3 independent experiments (27-65 cells per experiment) and expressed as the relative percentage of PBs compared to the transfection with wild-type DDX6 plasmid. Error bars, SD. (C) Complementation assays. As in Figure 4A, HeLa cells were first transfected with a siRNA targeting DDX6 (control) and 24 hours later with indicated FLAG-DDX6-HA plasmids named as in Figure 4. 40 h later, cells were analyzed by immunofluorescence using indicated antibodies. Bar = 10 μ m. Below is shown the number of PBs per cell (33-52 cells) expressed as the relative percentage of PBs compared to the complementation with wild-type DDX6 plasmid. Error bars, SD; t-test: $p < 0.0001$ for all mutants, as compared to wild-type.

Subject	Gene	Genomic Coordinates (GRCh37)	Variant	Inheritance	ACMG Classification	gnomAD het/hom count
S1	DDX6	chr11:118627025:C:T	NM_004397.5: c.1118G>A (p.Arg373Gln)	<i>de novo</i>	Likely Pathogenic	0 / 0
	DNAH11	chr7:21721269:G:A	NM_001277115: c.5449G>A (p.Val1817Met)	compound heterozygous	Uncertain Significance	21 / 0
		chr7:21932167:C:T	NM_001277115: c.12653C>T (p.Pro4218Leu)		Uncertain Significance	379 / 0
S2	DDX6	chr11:118626975:T:C	NM_004397.5: c.1168T>C (p.Cys390Arg)	<i>de novo</i>	Likely Pathogenic	0 / 0
S3	DDX6	chr11:118626972:T:G	NM_004397.5: c.1172C>T (p.Thr391Ile)	<i>de novo</i>	Likely Pathogenic	0 / 0
S4	DDX6	chr11:118626971:A:C	NM_004397.5: c.1171A>C (p.Thr391Pro)	<i>de novo</i>	Likely Pathogenic	0 / 0
	SLC16A2	chrX:73744603:G:A	NM_006517.4: c.985G>A (p.Ala329Thr)	hemizygous (maternal)	Uncertain Significance	0 / 0
S5	DDX6	chr11:118627028:T:C	NM_004397.5: c.1115A>G p.(His372Arg)	<i>de novo</i>	Likely Pathogenic	0 / 0

Table S1. List of variants initially considered for pathogenicity from WES /WGS studies of the cohort.

Gene name	Description	DE in S2
Eukaryotic translation initiation factor 3 family		
<i>EIF3A</i>	eukaryotic translation initiation factor 3, subunit A	-
<i>EIF3B</i>	eukaryotic translation initiation factor 3, subunit B	-
<i>EIF3C</i>	eukaryotic translation initiation factor 3, subunit C	up
<i>EIF3CL</i>	eukaryotic translation initiation factor 3, subunit C-like	-
<i>EIF3D</i>	eukaryotic translation initiation factor 3, subunit D	up
<i>EIF3E</i>	eukaryotic translation initiation factor 3, subunit E	-
<i>EIF3F</i>	eukaryotic translation initiation factor 3, subunit F	up
<i>EIF3G</i>	eukaryotic translation initiation factor 3, subunit G	-
<i>EIF3H</i>	eukaryotic translation initiation factor 3, subunit H	-
<i>EIF3I</i>	eukaryotic translation initiation factor 3, subunit I	-
<i>EIF3J</i>	eukaryotic translation initiation factor 3, subunit J	-
<i>EIF3K</i>	eukaryotic translation initiation factor 3, subunit K	-
<i>EIF3L</i>	eukaryotic translation initiation factor 3, subunit L	up
<i>EIF3M</i>	eukaryotic translation initiation factor 3, subunit M	-
Ribosomal protein family		
<i>RPL10</i>	ribosomal protein L10	up
<i>RPL10A</i>	ribosomal protein L10a	-
<i>RPL11</i>	ribosomal protein L11	-
<i>RPL12</i>	ribosomal protein L12	up
<i>RPL13</i>	ribosomal protein L13	up
<i>RPL13A</i>	ribosomal protein L13a	up
<i>RPL14</i>	ribosomal protein L14	-
<i>RPL15</i>	ribosomal protein L15	up
<i>RPL17</i>	ribosomal protein L17	-
<i>RPL18</i>	ribosomal protein L18	up
<i>RPL18A</i>	ribosomal protein L18a	-
<i>RPL19</i>	ribosomal protein L19	up
<i>RPL21</i>	ribosomal protein L21	-
<i>RPL22</i>	ribosomal protein L22	-
<i>RPL22L1</i>	ribosomal protein L22-like 1	-
<i>RPL23</i>	ribosomal protein L23	-
<i>RPL23A</i>	ribosomal protein L23a	up
<i>RPL24</i>	ribosomal protein L24	-
<i>RPL26</i>	ribosomal protein L26	-
<i>RPL26L1</i>	ribosomal protein L26-like 1	-
<i>RPL27</i>	ribosomal protein L27	-
<i>RPL27A</i>	ribosomal protein L27a	-
<i>RPL28</i>	ribosomal protein L28	up
<i>RPL29</i>	ribosomal protein L29	-
<i>RPL3</i>	ribosomal protein L3	up
<i>RPL30</i>	ribosomal protein L30	up
<i>RPL31</i>	ribosomal protein L31	-
<i>RPL32</i>	ribosomal protein L32	-
<i>RPL34</i>	ribosomal protein L34	-
<i>RPL35</i>	ribosomal protein L35	-
<i>RPL35A</i>	ribosomal protein L35a	up
<i>RPL36</i>	ribosomal protein L36	up
<i>RPL36A</i>	ribosomal protein L36a	-
<i>RPL36AL</i>	ribosomal protein L36a-like	-
<i>RPL37</i>	ribosomal protein L37	up
<i>RPL37A</i>	ribosomal protein L37a	-
<i>RPL38</i>	ribosomal protein L38	-
<i>RPL39</i>	ribosomal protein L39	-
<i>RPL39L</i>	ribosomal protein L39-like	-

<i>RPL4</i>	ribosomal protein L4	up
<i>RPL41</i>	ribosomal protein L41	-
<i>RPL5</i>	ribosomal protein L5	-
<i>RPL6</i>	ribosomal protein L6	-
<i>RPL7</i>	ribosomal protein L7	-
<i>RPL7A</i>	ribosomal protein L7a	up
<i>RPL7L1</i>	ribosomal protein L7-like 1	-
<i>RPL8</i>	ribosomal protein L8	-
<i>RPL9</i>	ribosomal protein L9	-
<i>RPLP0</i>	ribosomal protein, large, P0	-
<i>RPLP1</i>	ribosomal protein, large, P1	up
<i>RPLP2</i>	ribosomal protein, large, P2	up
<i>RPS10</i>	ribosomal protein S10	up
<i>RPS11</i>	ribosomal protein S11	up
<i>RPS12</i>	ribosomal protein S12	-
<i>RPS13</i>	ribosomal protein S13	-
<i>RPS14</i>	ribosomal protein S14	up
<i>RPS15</i>	ribosomal protein S15	up
<i>RPS15A</i>	ribosomal protein S15a	up
<i>RPS16</i>	ribosomal protein S16	-
<i>RPS17</i>	ribosomal protein S17	-
<i>RPS17L</i>	ribosomal protein S17-like	-
<i>RPS18</i>	ribosomal protein S18	-
<i>RPS19</i>	ribosomal protein S19	-
<i>RPS2</i>	ribosomal protein S2	-
<i>RPS20</i>	ribosomal protein S20	-
<i>RPS21</i>	ribosomal protein S21	-
<i>RPS23</i>	ribosomal protein S23	-
<i>RPS24</i>	ribosomal protein S24	-
<i>RPS25</i>	ribosomal protein S25	-
<i>RPS26</i>	ribosomal protein S26	-
<i>RPS27</i>	ribosomal protein S27	-
<i>RPS27A</i>	ribosomal protein S27a	-
<i>RPS27L</i>	ribosomal protein S27-like	-
<i>RPS28</i>	ribosomal protein S28	-
<i>RPS29</i>	ribosomal protein S29	-
<i>RPS3</i>	ribosomal protein S3	up
<i>RPS3A</i>	ribosomal protein S3A	-
<i>RPS4X</i>	ribosomal protein S4, X-linked	-
<i>RPS4Y1</i>	ribosomal protein S4, Y-linked 1	-
<i>RPS5</i>	ribosomal protein S5	up
<i>RPS6</i>	ribosomal protein S6	-
<i>RPS7</i>	ribosomal protein S7	up
<i>RPS8</i>	ribosomal protein S8	up
<i>RPS9</i>	ribosomal protein S9	up
<i>RPSA</i>	ribosomal protein SA	-

Table S3. Eukaryotic translation initiation factor 3 (eIF3) and ribosomal protein family genes differentially-expressed in Subject 2.